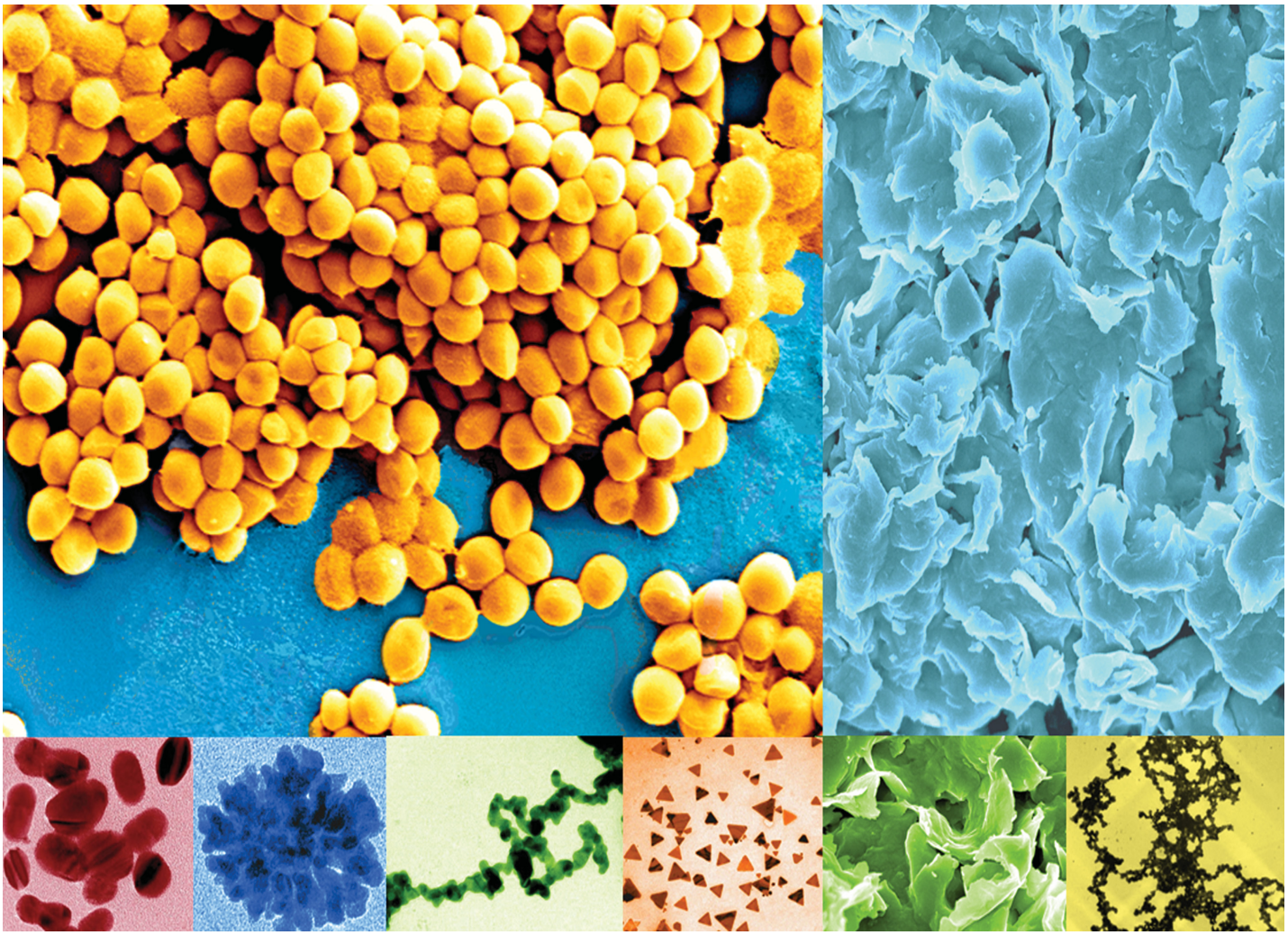

Showcasing research from Bioinspired Nanomaterials Laboratory of Dr Sujoy K. Das, CSIR-Indian Institute of Chemical Biology, Kolkata, India.

Nanotechnology based therapeutic approaches: an advanced strategy to target the biofilm of ESKAPE pathogens

Bacterial infections of ESKAPE pathogens cause major health risks. The emergence of antimicrobial resistance along with biofilm formation makes treatments more challenging. This review article highlights nanotechnology based therapeutic approaches utilizing nanomaterials as antibiofouling agents as well as delivery vehicles to disrupt the biofilm and killing of persister cells. This study also emphasizes the mechanism through which nanomaterials destroy biofilms and provide a deep insight into the potential application of nanomaterials in the biomedical field to cure biofilm associated infections of ESKAPE pathogens.

As featured in:

See Sujoy K. Das *et al.*, *Mater. Adv.*, 2023, **4**, 2544.

ROYAL SOCIETY OF CHEMISTRY

rsc.li/materials-advances

Registered charity number: 207890

Materials Advances

ROYAL SOCIETY OF CHEMISTRY

REVIEW

View Article Online
View Journal | View Issue

Cite this: *Mater. Adv.*, 2023, 4, 2544

Nanotechnology based therapeutic approaches: an advanced strategy to target the biofilm of ESKAPE pathogens

Arpita Mukherjee,[ab] Somashree Bose,[ab] Anirban Shaoo[a] and Sujoy K. Das *[ab]

Bacterial infection by ESKAPE (*Enterococcus faecium*, *Staphylococcus aureus*, *Klebsiella pneumoniae*, *Acinetobacter baumannii*, *Pseudomonas aeruginosa*, *Enterobacter* spp.) pathogens are one of the major health concerns and has caused a global crisis in the healthcare sectors, leading to mortality, morbidity, and socioeconomic loss. The overuse and abuse of antibiotics has led to an increased number of MDR bacteria. Thus, conventional antibiotics have failed to show notable improvement in bacterial infections. Biofilm formations make pathogens more recalcitrant than their planktonic form, and are becoming more challenging to treat with conventional antibiotics. To overcome the challenges of the biofilm-associated chronic infections of ESKAPE pathogens, a new therapeutic strategy is urgently needed. Recently, nanomaterial-based therapies have emerged as a novel approach to combat the biofilm infection of ESKAPE pathogens. The size, shape and other physicochemical properties of nanomaterials play a significant role in targeting the biofilm and overcoming the recalcitrant bacterial infection. Herein, we give a brief review about the formation and structure of biofilms of ESKAPE pathogens and the quorum-sensing (QS) mechanism in biofilm formation. Subsequently, we discuss the conventional methods and strategies for the treatment of biofilms and their limitations. Later, we highlight different strategies for the fabrication of nanoparticles, which include solid nanoparticles, conjugated nanoparticles and nanocarrier systems that can be used to target the bacterial biofilm. We also discuss different interaction mechanisms through which nanoparticles disrupt the biofilm and kill the sessile and persister cells. Therapeutic applications of nanomaterials in biomedical fields are also systematically reviewed. Lastly, we discuss the current status and future perspectives of nanotechnology. We believe that this article provides insights into the advancement of nanotechnology, and offers an alternative therapeutic strategy to treat biofilm-associated infections.

Received 29th July 2022,
Accepted 20th March 2023

DOI: 10.1039/d2ma00846g

rsc.li/materials-advances

1. Introduction

ESKAPE pathogens are one of the major causes of nosocomial infections, and account for 2 million illnesses and 23 000 deaths per year as per the reports of Centers for Disease Control and Prevention (CDC).[1] Bacterial colonization and successive biofilm formation by ESKAPE pathogens are a major threat in the biomedical sector. The bacterial cells in the biofilm are surrounded by extracellular polymeric substances (EPS), which provide structural stability and protect the cells from harsh environmental conditions.[3,4]

It has been reported that the formation of a biofilm makes the bacteria 1000 times more antibiotic-resistant compared to their planktonic ones because EPS hinders the penetration of antibiotics.[2,5] EPS accounts for 50%–90% of the total biomass of biofilms, thereby inhibiting the penetration of antimicrobials.[6] QS[7] plays a pivotal role in the initiation, development, and maturation of biofilms, as well as the release of planktonic bacteria from it. Autoinducers secreted by the pathogens help in cell-to-cell communication, which is further involved in biofilm formation, expression of pathogenic factors and evading host immunity. Besides that, the altered pH of the biofilm inactivates the antibiotics and helps the bacteria to survive in harsh environmental conditions.[2,3,7]

The abbreviation ESKAPE represents six groups of pathogens, *i.e.*, *Enterococcus faecium*, *Staphylococcus aureus*, *Klebsiella pneumoniae*, *Acinetobacter baumannii*, *Pseudomonas aeruginosa* and *Enterobacter* spp.[4] The ESKAPE pathogens are named due to their escaping strategies from known antibiotics, including the penicillin group of drugs, carbapenemase, vancomycin, and even colistin, making them multi-drug resistant. Many

[a] *Infectious Diseases and Immunology Division, Council of Scientific and Industrial Research (CSIR)-Indian Institute of Chemical Biology, Kolkata-700032, India. E-mail: sujoydas@iicb.res.in, sujoydasiacs@gmail.com; Tel: +91 33 24995 905*
[b] *Academy of Scientific and Innovative Research (AcSIR), Ghaziabad-201002, India*

conventional approaches, such as physical and chemical-based strategies, exist for the treatment of biofilm-related infections by ESKAPE pathogens. Different therapeutic strategies, such as antibiotics, antimicrobial peptides, polymers and polysaccharides, are also used to treat the bacterial biofilm-related infections. Extensive utilization of antibiotics leads to the generation of MDR bacteria, which reduces the efficacy of the antibiotics.[1,2] Bacteria inside the biofilm are prone to high mutation rates and interchangeable resistant genes on transposable elements, leading to the overall resistance to the cells of biofilm. Moreover, the above-mentioned strategies are expensive, requiring multiple doses with uncertain and adverse outcomes.[4,7]

Arpita Mukherjee

Arpita Mukherjee is presently pursuing her PhD at the Infectious Diseases and Immunology Division, Council of Scientific and Industrial Research- Indian Institute of Chemical Biology (CSIR-IICB), Kolkata, India under the supervision of Dr Sujoy K. Das, Principal Scientist at CSIR-IICB. She completed her graduation from Hooghly Women's College, The University of Burdwan, Bardhaman, West Bengal, India, majoring in Microbiology in 2017. She received her MSc degree from The University of Burdwan, Bardhaman, West Bengal, India, majoring in Microbiology in 2019. Her research focus is on the development of surface-engineered nanoparticles for application in the eradication of bacterial biofilms.

Somashree Bose

Somashree Bose received her BSc degree from Acharya Prafulla Chandra Roy Government College, University of North Bengal in 2015, majoring in Zoology. Then, she completed her MSc studies from Ranchi University in 2017, majoring in Zoology. She is currently pursuing her PhD degree at the Infectious Diseases and Immunology Division, CSIR-IICB, Kolkata, India under the supervision of Dr Sujoy K. Das. Her research focus is on the development and application of smart transdermal scaffolds as novel drug delivery systems to combat bacterial infections and accelerate wound healing. She is a coauthor of one research paper in an international journal of high repute, and has also filed a patent from India.

Anirban Shaoo

Anirban Shaoo received his BSc degree from Asutosh College, University of Calcutta, Kolkata, West Bengal, India in 2017, majoring in Biochemistry. Subsequently, he successfully completed his post-graduate studies in 2019 at Ballygunge Science College, University of Calcutta, Kolkata, West Bengal, India, majoring in Biochemistry. Currently, he is working as a Project JRF under the supervision of Dr Sujoy K. Das at the Infectious Diseases and Immunology Division, CSIR-IICB, Kolkata, India. His research focus is on the photothermal ablation of bacterial infections with the help of 3D hydrogels.

Sujoy K. Das

Dr Sujoy K. Das, Principal Scientist, CSIR-Indian Institute of Chemical Biology, India and Associate Professor of Academy of Scientific and Innovative Research (AcSIR), New Delhi, India. He is a Fellow of the Royal Society of Chemistry (FRSC), UK, and a Fellow of the Academy of Sciences Chennai (FASCh), India. Dr Das obtained his PhD degree from the Indian Association for the Cultivation of Science. He pursued his postdoctoral research studies at Dublin City University, Ireland and Technical University, Dresden, Germany. His research interests are broadly focused on the design and synthesis of bioinspired nanomaterials, delivery of antimicrobial peptides for the inhibition and disruption of bacterial biofilms, and smart hydrogel fabrication and photodynamic therapy for wound infection management. He has published more than 50 research articles (>5200 citations, h-index 36) in peer-reviewed journals, and has two patents in his credit. He also filed two patents and contributed to two book chapters. He is an Editorial Board Member of Enzyme and Microbial Technology, and edited a special issue as a Guest Editor.

Recently, nanotechnology has emerged as a promising alternative to the conventional approaches for the effective treatment of bacterial biofilms. Nanomaterials having dimensions in the range of 1 to 100 nm possess unique physicochemical properties, such as small size, increased surface area-to-volume ratio, and increased thermal, electrical, optical and magnetic properties.[8] Metal and metal oxide nanomaterials often act as antimicrobial agents due to their biotic interaction with microbes, which inhibits and disrupts the biofilm. Apart from that, nanomaterials like lipids, polymers, and micelles, also act as vehicles to deliver antimicrobial agents owing to their very small size and better penetration property within the biofilm matrix.[9–11] In this review, we give a summary of the formation and structure of the biofilms of ESKAPE pathogens and their QS mechanism associated with the biofilm formation. Next, we highlight the efficacy of various nanomaterials based on different approaches to inhibit bacterial biofilm formation and disruption of the mature biofilm. Different treatment strategies use nanoparticles such as metal-based, carbon-based, 2D nanoparticles, nanoemulsions, lipid-based and several polymeric nanoparticles for removing biofilm. We also discuss the application of various nanomaterials such as metals, carbon, lipids and polymers in various biomedical fields to combat biofilm-related bacterial infections. Finally, we illustrate the current status and future perspective of nanotechnology for the effective treatment of ESKAPE pathogens. We believe that this review will give a brief idea to understand the development of nanomaterials as a promising antibacterial and antibiofouling agent to fight against chronic biofilm-related infections.

2. Biofilm formation and QS system of ESKAPE pathogens

Biofilms are heterogenous, multicellular surface-adhered sessile microbial communities surrounded by an EPS matrix, which consist of less than 10% dry weight of the microorganism and 90% dry weight of its matrix.[12] The EPS of the biofilm contains exopolysaccharides, eDNA, lipids, proteins and other macromolecules. The EPS of the biofilm acts as a protective barrier, serving as the storage of nutrients. Biofilm formation takes place in four stages, such as surface attachment, biofilm formation, maturation and dispersal (Scheme 1).[13–15]

(1) Surface attachment

Microbial cells attach to the surfaces through various interactions, such as van der Waals, electrostatic and hydrophobic interactions, and become sessile.[16] Capsular polysaccharide/adhesion (PS/A), fimbriae, pilus-like structures play a key role in the initial attachment of the bacteria to the surfaces.[13]

(2) Biofilm formation

The surface-attached cells rapidly divide to form micro-colonies and secrete EPS, leading to the formation of a biofilm matrix.[17]

(3) Biofilm maturation

In this stage, the biofilm forms a three-dimensional (3D) structure that provides structural stability and protects the cells from chemicals, host defense and harsh environmental conditions.[17] Matured biofilms have dormant bacterial subpopulations called persisters, and show high tolerance to antibiotics.[18]

(4) Dispersal of biofilm

The cells inside the biofilm detach from the substratum and go to a different location.[13]

During biofilm formation, cell-to-cell communication takes place by a signaling process called QS. It plays a vital role in maintaining pathogenicity of the bacteria by controlling different virulent genes, which are required for the formation of the biofilm.[7] The Gram-positive bacteria release small peptides named autoinducing peptides (AIP), while Gram-negative bacteria release a chemical called acyl-homoserine lactone (acyl-HSL) into the extracellular environment, and communicate with each other.[19] After reaching a threshold concentration, these QS molecules (AIP and acyl-HSL) are recognized by the surrounding bacterial cells. These QS molecules bind to the specific receptor kinase of the cells, which further activates other sensory kinases and regulates the expression of different genes related to biofilm formation and pathogenesis.[19,20]

E. faecium is one of the common nosocomial pathogens that causes biofilm-mediated infection and becomes difficult to treat. Autolysin in *E. faecium*, named AtlAEfm, is involved in the stability of the biofilm. Among several virulence genes, enterococcal surface protein (Esp) and enterococcal biofilm regulator B (EbrB) take part in biofilm formation.[21,22] Secretion of these virulence factors in *E. faecium* is regulated by the Fsr QS system.[23] *S. aureus* secretes glycocalyx-containing materials, which form a multilayered biofilm where heterogeneous protein expression occurs throughout the biofilm. EPS of *S. aureus* contains polysaccharide intracellular antigen (PIA), which is involved in the regulation of *Staphylococcal* biofilm formation.[24] Biofilm-associated protein (Bap), surface-associated proteins such as protein A, fibrinogen binding proteins (FnBPA and FnBPB), *S. aureus* surface protein (SasG), and clumping factor B (ClfB) are important components for the attachment and development of the biofilm matrix. There are some secreted proteins like extracellular adherence protein (Eap) and beta toxin (Hlb), which help in the maturity of the *Staphylococcal* biofilm.[25,26] The accessory gene regulator (agr) locus regulates the QS system, and is thus involved in the biofilm formation in *S. aureus* (Scheme 2A). AgrA and AgrC comprise the two component regulatory system, which senses the autoinducing cyclic octapeptide. The peptide is processed by AgrB, which is the product of agrD.[27,28] Like other Gram-negative bacteria, *K. pneumoniae* (Scheme 2B) does not secrete acyl-HSLs AHL. Rather, it encodes SdiA (suppressor of the cell division inhibition), an orphan LuxR type receptor that responds to acyl-HSLs AHLs of other species. *K. pneumoniae* secretes different virulence factors like capsule polysaccharide,

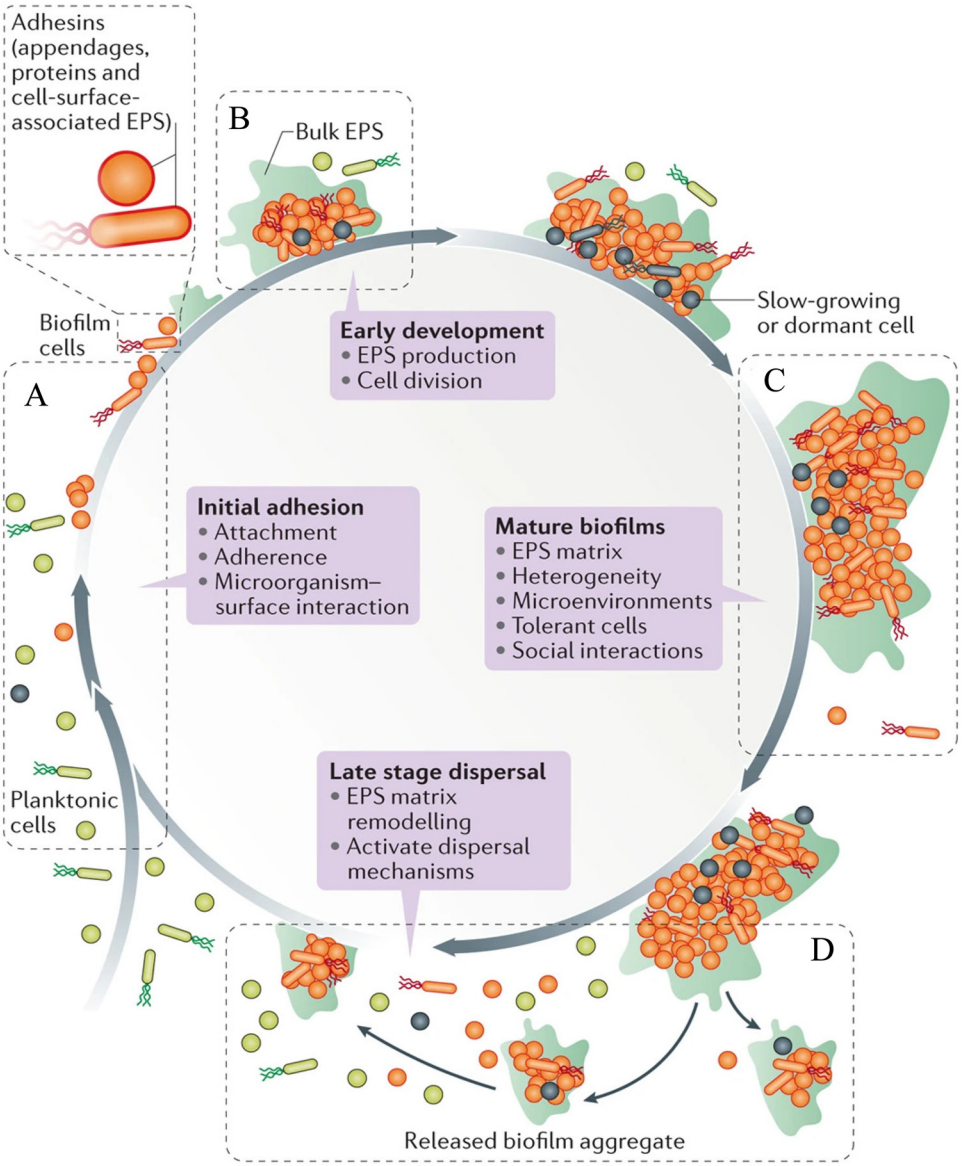

Scheme 1 Various stages of the biofilm life-cycle comprising (A) surface attachment, (B) biofilm formation, (C) biofilm maturation and (D) dispersal of biofilm. Reprinted with permission from ref. 46.

lipopolysaccharide (LPS), type 1 and type 3 fimbriae, which help to establish infection by evading the host immune system and biofilm formation.[29–31] Type 3 fimbriae and capsular polysaccharide are the most important factors in biofilm establishment, where fimbriae mediate stable adherence and capsular polysaccharide is involved in cell-to-cell communication and biofilm structure formation.[32] The biofilm formation of *A. baumannii* involves outer membrane protein A (OmpA), chaperon-usher pilus (Csu), biofilm associated protein (Bap), EPS, and poly-β-(1,6)-*N*-acetyl glucosamine (PNAG). OmpA facilitates *A. baumannii* to attach and invade the epithelial cell, and contribute to drug resistance and biofilm formation.[33] Bap is a large surface exposed protein homologous to *S. aureus*, which is involved in cell–cell interaction and helps in adherence.[34] The luxR/luxI type QS locus is called abaR/abaI in *A. baumannii* (Scheme 2C). The abaI gene encodes a 183 amino acid protein, which is involved in signal transduction, whereas abaR encodes a 238 amino acid protein, which acts as the autoinducer synthase receptor.[35–37] Psl (polysaccharide synthesis locus), Pel (pellicle) and alginate are the three exopolysaccharides secreted by *P. aeruginosa*, where Psl helps to attach the cells to the surfaces, and is involved in cell–cell communication. It also helps to maintain the structural stability of the biofilm by presenting the periphery of the biofilm matrix. Pel is an important matrix component responsible for the surface attachment and structural stability of the biofilm, providing resistance against aminoglycoside antibiotics to the biofilm. Alginate plays a vital role in biofilm maturation, evading phagocytosis, opsonization and reducing antibiotic diffusion through the biofilm.[38–40] Two complete acyl homoserine

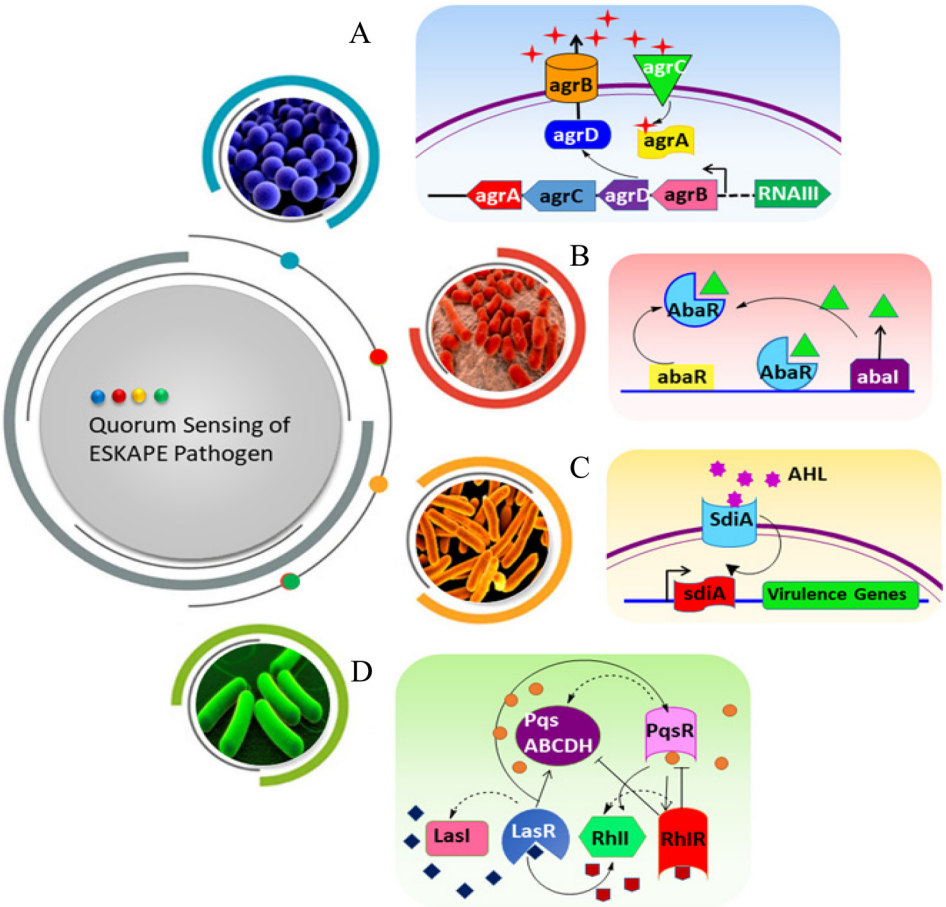

Scheme 2 QS pathway of ESKAPE pathogens. (A) *S. aureus*, (B) *A. baumanni*, (C) *K. pneumoniae* and (D) *P. aeruginosa*.

lactone systems are found in *P. aeruginosa* (Scheme 2D), named as the LasR-LasI and RhlR-rhlI system. LasI produces *N*-3-oxo-dodecanoyl-homoserine lactone (3OC12-HSL), while RhlI produces *N*-butanoyl-homoserine lactone (C4-HSL). LasR and RhlR are two transcription factors that are activated by 3OC12-HSL and C4-HSL, respectively, and regulate the transcription of different genes related to bacterial pathogenesis. The expression of several virulence factors like pyocyanin, elastase and exotoxin help in the development of biofilms in *P. aeruginosa*.[41–43] Among *Enterobacter* spp., *Enterbacter cloacae* is mainly involved in biofilm-related infections. T6SS-2 of *E. cloacae* exhibits a vital role in the formation of biofilms, and also helps in attaching the bacteria to eukaryotic cells.[44] This QS pathway can be disrupted by different mechanisms, such as (i) reducing the activity of receptors, (ii) inhibiting the synthesis of QS molecules (acyl-HSL, AIP), (iii) degradation of QS molecules, and (iv) mimicking of the signaling molecules.[45]

3. Existing strategies for biofilm inhibition and disruption

There are many existing strategies implemented for biofilm management in health care sectors, which include physical, chemical, drugs and other molecules. Scheme 3 illustrates three types of existing strategiesm and their limitations in biofilm inhibition and disruption. The physical method includes mechanical disruption of the biofilm by scrubbing, shear stress like jet spray, brushes, electric waves including ultrasound, laser shock, and UV rays, leading to the removal of the biofilm layer from the surgical instruments, hospital floors, bed, and others.[46,47] On the other hand, different sprays and water-based jets are mostly used to eradicate the dental and surgical biofilms, and thus remove the dead necrotic tissue and exudates often referred to as debridement. The combination therapy of antibiotics along with debridement of the dead necrotic tissue could also be applied as a therapeutic strategy for curing bacterial infection.[48]

The chemical-based antibiofilm agents involve the utilization of antimicrobial disinfectants, namely hydrogen peroxide (H_2O_2),[49,50] chlorine-based chemicals (sodium hypochlorite, hypochlorous acid), surfactant-based chemicals, quaternary ammonium compounds, povidine-iodine and chlorhexidine gluconate.[46] Among all these antimicrobial agents, H_2O_2, HOCl and HOBr are strong oxidants that attack the cellular membrane lipids, DNA and other cellular contents, and effectively kill the microorganism. In the presence of hydrogen peroxide and chloride/bromide ions, vanadium

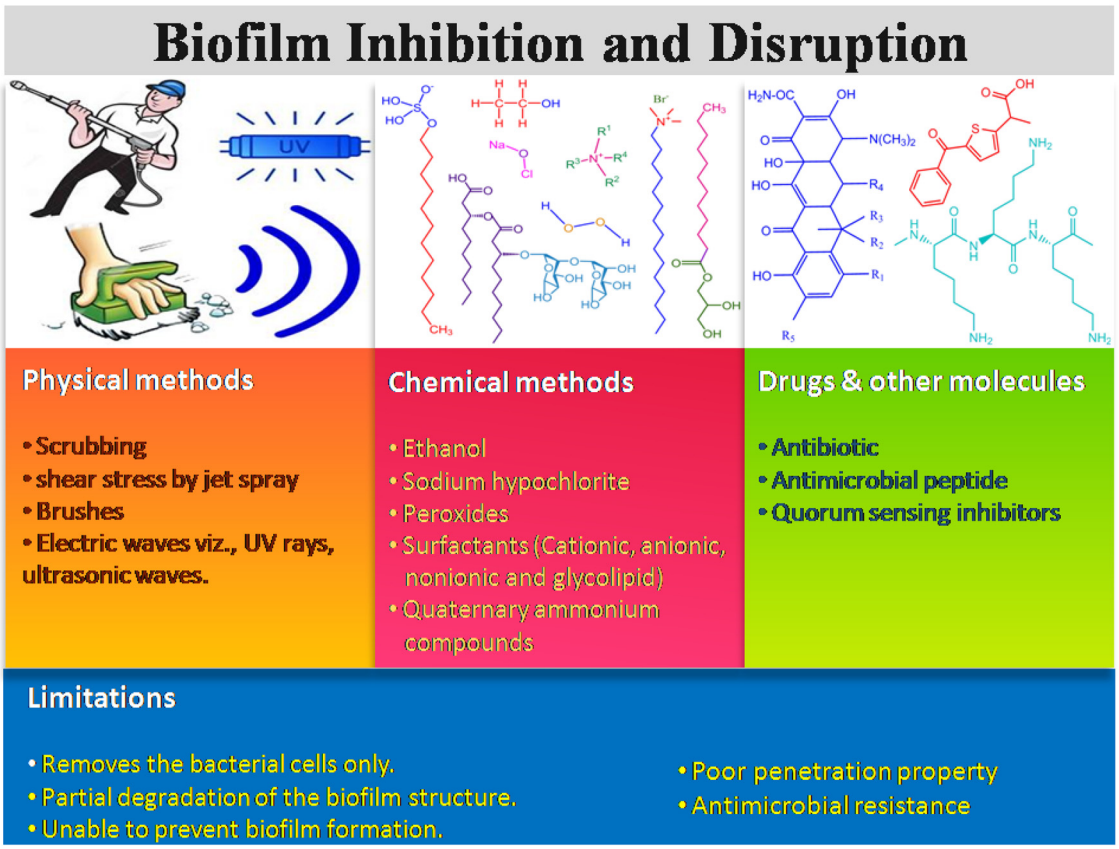

Scheme 3 Conventional approaches for biofilm inhibition and disruption.

haloperoxidases have been reported to form HOCl/HOBr, which acts as a strong bactericidal and oxidizing agent against *P. aeruginosa* biofilms.[51] QACs kill the microbes by cleaving their cell membrane, leading to nutrient efflux and hence cell lysis.[52,53] Gemini QAC shows antibacterial and antibiofouling activities against *P. aeruginosa*.[54] QACs are used in the cleaning of chronic wound infections. Different ionic and non-ionic surfactants are also conventionally used to inhibit and disrupt the biofilm formation.[55–57] Surfactants usually weaken the EPS matrix, which causes surface detachment, leading to biofilm disruption. Apart from this, phage therapies (KPP10 against *P. aeruginosa*,[58] ABSA01 phage cocktail against MRSA,[59] pIsf-AB02 against MDR *A. baumannii*[60]) against bacterial biofilms have also been developed.

Different small molecules, like antibiotics, antimicrobial peptides, and QS inhibitors with known antimicrobial activities, are used for treating the biofilm infections caused by ESKAPE pathogens.[61,62] Antibiotics are still considered the best therapeutic agent to kill the bacterial cells through different modes of action, such as inhibition of DNA replication, cell wall synthesis, protein synthesis and various metabolic processes. Antibiotics like aztreonam, tobramycin and vancomycin serve as an antibiofouling agent and disrupt the biofilm formation through inhibition of filamentation, peptidoglycan biosynthesis, and affecting the bacterial cell permeability.[63,64] The antimicrobial peptides (AMPs) have been explored as an alternative antibiofouling agent in the biomedical field. It has been reported that TAT-RasGAP317-326 with TAT HIV 48-57 sequence[65] and AMP 1018-K6[66] exhibit antibiofilm properties, and inhibit the biofilm formation of *P. aeruginosa*, *A. baumannii, S. aureus* and methicillin resistant *S. aureus* (MRSA), respectively. Moreover, there are several limitations of these conventional techniques. Physical strategy causes the physical removal of the biofilm through aggressive debridement, but a few populations of sessile bacteria still remain on the surfaces. After completion of the treatment, the remaining bacterial cells act as a nucleation point and the biofilm repopulation takes place. For example, shear stress disturbs the biofilm integrity, but it fails to kill the persister cells.[46] The antibiotics, antimicrobial peptides, QS inhibitors also have strong limitations, such as their reduced uptake into the biofilm matrix due to the protective EPS layer, inactivation by low pH, and anoxic condition of the biofilm, enzymatic degradation and/or their modification inside the biofilm microenvironment.[2,67] Therefore, it is necessary to explore an alternative process and/or materials for effective dispersal of the bacterial biofilm.

4. Nanotechnology-based approach to combat biofilm

The emergence of nanoscience and nanotechnology provides an opportunity to deal with the biofilm of ESKAPE pathogens in

an effective manner. Owing to their small size, large surface area and high surface-active groups, nanomaterials exhibit unique physicochemical properties. These physicochemical properties can be further tuned by varying the morphology (size and shape of the particles) and surface modifications of the nanoparticles.[68] Nanoparticles act either as an antibacterial and antibiofouling agent, or as a smart carrier for the effective delivery of the antimicrobial agent/drugs inside the biofilm matrix.[69] The nanotechnology-based approaches can be classified into three categories (Scheme 4): (1) solid nanoparticles, (2) conjugated nanomaterials and (3) nanocarrier system. The solid nanoparticles mainly focus on the utilization of inorganic nanoparticles, carbon-based, dendrimer and polymeric nanoparticles to inhibit and disrupt the biofilm formation.[70–72] In the conjugated nanomaterials system, the solid nanoparticles are further functionalized with polymers, peptides and different bioactive molecules to increase the efficacy of the nanoparticles to disrupt the biofilm formation.[73,74] In the nanocarrier system, nanomaterials have been explored to deliver the drugs, antibiotics, peptides and other small molecules to inhibit and disrupt the biofilm formation. Nanoparticles are also reported to play a role in breaking the QS system. Interference with the QS activity is an excellent strategy to inhibit bacterial pathogenicity without increasing the resistance among the bacteria. Some nanoparticles like AgNPs,[75] SeNPs,[76] and ZnO NPs[77] show anti-QS activity against ESKAPE pathogens. They interfere with the AHL production, down-regulate luxA and luxR, and attenuate the secretion of several virulence factors mediated by the QS system.

4.1. Inorganic nanoparticles and nanomaterials

Inorganic nanoparticles include a wide range of materials; namely, elemental metals, metal oxides, dichalcogenide, and others.[78] Owing to their unique physicochemical properties, inorganic nanomaterials are widely used as antimicrobial and antibiofilm agents. The bactericidal action of the inorganic nanoparticles involves the alteration of the membrane potential, cell membrane damage, leakage of the cytosolic contents, generation of reactive oxygen species (ROS), oxidative stress and metabolic inactivation.[79] Inorganic nanoparticles have also been modified by functionalization with different types of target specific molecules, like antimicrobial peptides and/or polymers. Some inorganic nanoparticles have also been explored as a nanocarrier to deliver different antibiotics and antimicrobial agents.

4.1.1. Metal nanoparticles. Metal nanoparticles, such as gold, silver, copper, selenium, platinum and others, interact with the bacterial cell membrane, leading to disruption of the cell. Metal ions released from these nanoparticles can also play a significant role in the bactericidal mechanism. The leached

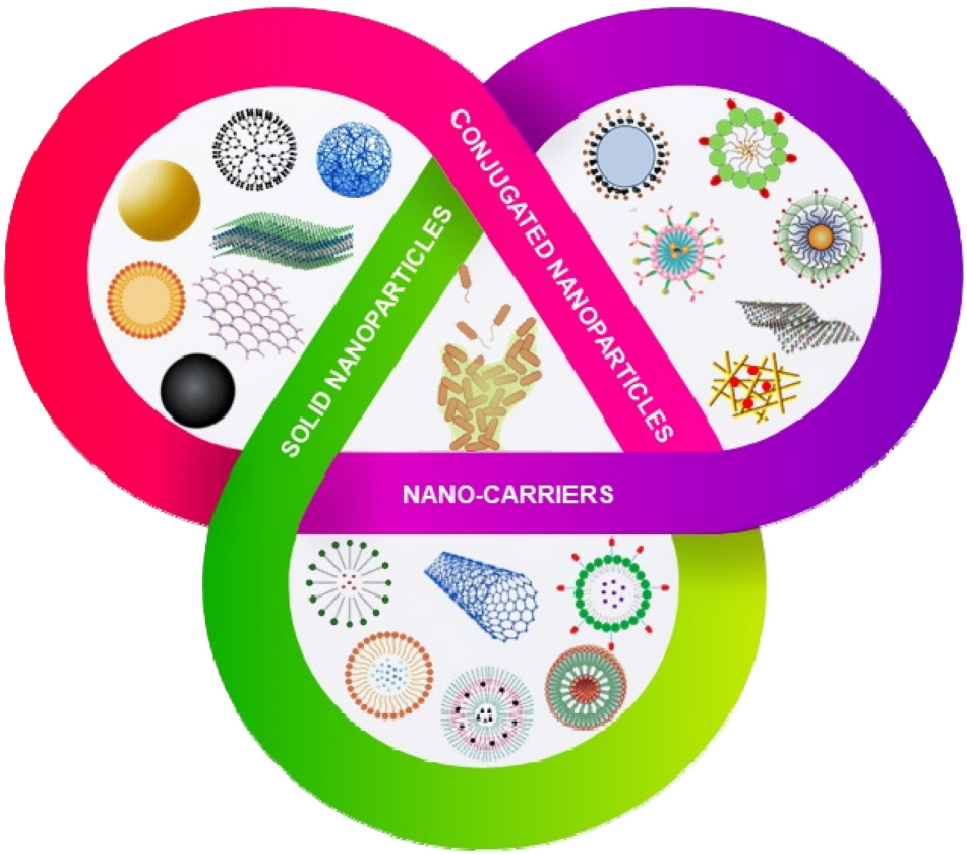

Scheme 4 Nanotechnology based approaches to eradicate biofilms. Nanomaterials can be classified as solid nanoparticles, conjugated nanoparticles and nanocarrier systems.

metal ions enter the cell and disrupt biological processes. Beside these, metal nanoparticles produce oxidative stress-mediated ROS, which hampers cellular functions and metabolic activities of the cells, leading to the cell death.[80]

Among different nanoparticles, silver nanoparticles (AgNPs) are considered one of the best antimicrobial metal nanoparticles.[81] AgNPs have strong antibacterial and antibiofilm activity through binding with the cell wall of bacteria and damaging the cell membrane, causing leakage of the intracellular components, including proteins and nucleic acids.[82] A 23%–86% biofilm inhibition of the *K. pneumoniae* strain was observed in the presence of different concentrations of AgNPs. Some other studies demonstrated that AgNPs disrupt the microbial membrane by leaching the Ag^{+} ions.[83] To explore the antibiofilm property of gold nanoparticles (AuNPs), Qiao *et al.*[84] functionalized gold nanorods (AuNRs) with NIR light-responsive and pH-activated surface charge changeable polymethacrylate having carboxyl betaine groups by reversible addition-fragmentation chain transfer polymerization reaction. The pH-responsive charge transformations led to the killing of the planktonic cells. Photothermal NIR irradiation causes local hyperthermia, leading to the death of *S. aureus* and consequently biofilm disruption (Fig. 1A). Khan *et al.*[85] functionalized antibacterial fucoidan to stabilize AuNPs, which hampered the preliminary adhesion of the planktonic cells, thus inhibiting the biofilm formation. This conjugate also disintegrated the mature *P. aeruginosa* biofilm. Metal nanoparticles also act as a novel delivery system, wherein the *P. aeruginosa* PAO1 biofilm was disrupted and eliminated from the lungs of mice by a silver nanosystem (Ag@MON-AE) carrying AgNPs and a mesoporous organosilica layer for the delivery of alginate lyase and ceftazidime (Fig. 1B).[86] Transmission electron microscopy (TEM) and scanning electron microscopy (SEM) images of Ag@MON-AE showed an alginate lyase-loaded Ag nanocomposite. The Ag@MON-AE nanocomposite showed 73.71% biofilm degradation at pH 6.4. The acidic environment of the biofilm increased the activity of alginate lyase, and was responsible for the release of ceftazidime. The synergistic activity of silver, alginate lyase and ceftazidime demonstrated the high biofilm degradation of PAO1. In another study, Wang *et al.*[87] fabricated a multilayered film that consisted of gentamicin, tannic acid and silver nanoparticles coated on magnetic nanoparticles. The magnetic nanoparticles were further coated with hyaluronic acid to make it biocompatible.

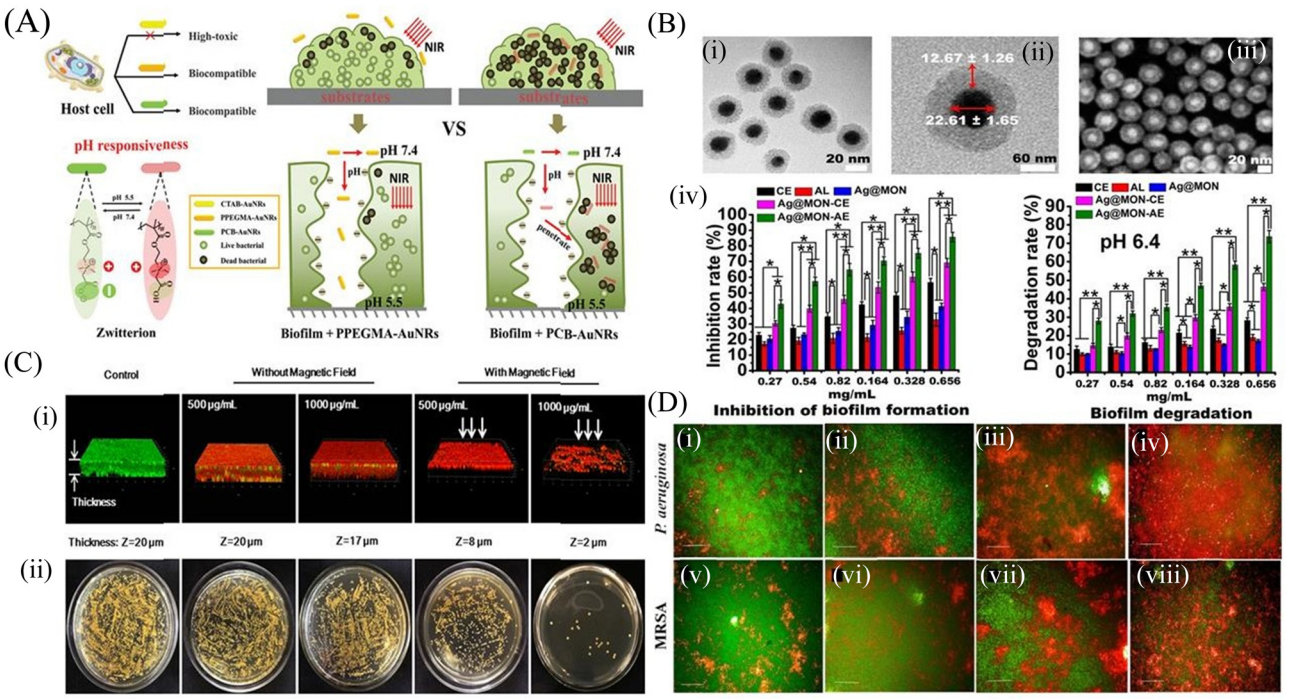

Fig. 1 Inorganic nanomaterials: (A) Illustration of gold nanorods with charge-switchable properties and their interactions with mammalian cells and biofilms. (B) Characterization of the Ag@MON nanoparticles: (i) TEM image of the silver nanoparticles coated with mesoporous organosilica, (ii) Structural characteristics of Ag@MON at TEM magnification, (iii) SEM image of Ag@MON, (iv) Restraining and degrading the biofilm formed by *P. aeruginosa* PAO1. *P. aeruginosa* PAO1 was incubated with different concentrations of PBS, AL (alginate lyase), CE (ceftazidime), Ag@MON, Ag@MON-CE, and Ag@MON-AE for 36 h at 37 °C in a 96 well plate. The biofilm formed by the bacteria was determined. In addition, the ability of the compounds to degrade the biofilm formed by *P. aeruginosa* PAO1 after culturing for 72 h was analyzed under a pH 6.4 condition. (C) (i) Live/Dead staining of 3-D reconstructions of z-stacks collected across the *S. aureus* biofilms, and (ii) Bacterial colonies of surviving *S. aureus* in biofilms after treatment with MNPs@Ag@HA without and with an applied magnetic field (NdFeB, 2000 Gauss), respectively. (D) Membrane integrity assessment of preformed biofilms live and dead cells differentiated SYTO 9 and PI-stained *P. aeruginosa* and MRSA biofilms with treatment combinations: (i and v) Control biofilms without treatment, (ii and vi) Biofilms treated with LP alone, (iii and vii) Biofilms treated with CuNPs alone, (iv and viii) Biofilms treated with LP + CuNPs (50 μM). (A) Reprinted with permission from ref. 84. (B) Adapted with permission from ref. 86. (C) Reprinted with permission from ref. 87. (D) Reprinted with permission from ref. 88.

The nanocomposite could permeate through the *S. aureus* and *E. coli* biofilm by their magnetic field navigation, and exhibited strong antibiofilm and antibacterial efficacy. High ROS production in the presence of the magnetic field caused decomposition of the biofilm matrix, and finally led to the removal of the biofilm. Fig. 1C shows the confocal images of the control *S. aureus* biofilm, and the biofilm with and without a magnetic field. After the application of the magnetic field, the biofilm structure started to disintegrate and bacterial cells started to die. A copper nanoparticles (CuNPs)-encapsulated liposomal formulation was prepared to increase the effectiveness of the lipopeptide biosurfactant.[88] The as-prepared nanoformulation reduces the cellular metabolism, and also influences the secretion of different virulence factors of MRSA and *P. aeruginosa*. High content screening (HCS) imaging of the biofilm using SYTO 9 and PI demonstrated that EL-LP-CuNP had immense killing efficiency at $\frac{1}{2}$ MIC concentrations against both *P. aeruginosa* and MRSA (Fig. 1D).

4.1.2. Metal oxide nanoparticles. Metal oxide nanoparticles such as CuO, ZnO, MgO, TiO_2, Al_2O_3, and Fe_3O_4 show biofilm inhibition and disruption properties by (a) causing mechanical damage to the cell wall, (b) generation of ROS through oxidative stress, and (c) disruption of cellular machineries due to the release of metal ions.[89–91] Copper oxide (CuO) nanoparticles disrupt the cellular machinery and biochemical process to specific sites of the DNA, and generate numerous OH^- radicals around the binding site. This results in various damages in nucleic acids. The CuO nanoparticles showed four types of reactive oxygen that inhibited biofilm formation and eradicated the matured biofilm.[92] Due to its antibacterial and antibiofouling activity, titanium dioxide (TiO_2) nanoparticles were explored as a coating material to prevent the biofilm formation. Altaf *et al.*[93] synthesized TiO_2 nanoparticles and coated them on the glass surfaces. TiO_2 interferes with the bacterial attachment and colonization of bacteria onto the glass surface, and inhibits the EPS secretion of the biofilm in a dose-dependent manner (Fig. 2A). Light microscopic images of biofilms of *E. coli* ATCC 25922, *P. aeruginosa* PAO1 and *S. aureus* MTCC 3160 showed significant inhibition at 64 μg mL^{-1} of TiO_2 NPs, whereas a heavily colonized glass surface was observed in the case of untreated biofilms. A remarkable change in the biofilm's architecture was observed under SEM after treatment with TiO_2 NPs, which further confirmed the inhibition and eradication of biofilms. Treated *S. aureus* biofilms showed lower amounts of biofilm and reduced bacterial colonization, which was the same as that for the *P. aeruginosa* biofilm. These nanoparticles reduced the biofilm-forming capability of *P. aeruginosa*, as well as *S. aureus*. In contrast, the untreated *S. aureus* and *P. aeruginosa* exhibited high loads of bacteria on the glass surface. In the case of *E. coli*, it was found that around 70% reduction of the biofilms of bacteria was observed by TiO_2. Metal oxide nanoparticles like Fe_3O_4 nanoparticles release Fe^{2+}, which reacts with oxygen to form hydrogen peroxide, leading to the generation of ROS through the Fenton reaction.[94,95] NO is an effective regulator of biofilms, but the by-products produced from NO generators are unstable and nonspecific to the target site. Metal oxide nanoparticles also act as a delivery vehicle of NO to disrupt the biofilm biomass. In a study, Adnan *et al.*[96] demonstrated that polydopamine (PDA)-coated iron oxide nanoparticles (IONPs) conjugated with a hydrophilic polymer to load NO gas caused biofilm reduction up to 79%. The PDA-functionalized IONPs were synthesized by the Michael addition reaction, as shown in Fig. 2B. They prepared two formulations: PDA-coated IONP called IONP@PDA-NO and a block copolymer P(OEGMA)-*b*-P(ABA) conjugated IONP@PDA denoted as IONP@PDA-HP-NO. IONP@PDA-NO and IONP@PDA-HP-NO induced dispersal of the *P. aeruginosa* biofilm at and above 1.5×10^{-6} M concentration. A crystal violet staining of the biofilm biomass showed a reduction of 72% and 70% of the *P. aeruginosa* biofilm by IONP@PDA-NO and IONP@PDA-HP-NO, respectively, in comparison to the untreated control. Even at a very low concentration of NO like 0.375×10^{-6} M, IONP@PDA-HP-NO exhibited strong dispersal of the biofilm. This resulted in biofilm biomass reduction by 79%. In contrast, at the same NO concentration, IONP@PDA-NO could not induce dispersal of the biofilm biomass. As a control, they used an equivalent amount of PDA-coated nanoparticles to observe the dispersal of the biofilm. However, the nanoparticles failed to exhibit a significant amount of biofilm dispersion, which proved that the antibiofilm activity of the nanoparticle was due to the release of NO.

Some of the nanoparticles are reported to inhibit QS within the bacterial population. Khan *et al.*[97] explored the antibacterial and antibiofilm efficacy of zinc oxide nanospikes (ZNs), *i.e.*, ZN1 and ZN2, against the biofilm of *P. aeruginosa* (PAO1). ZNs prevented the QS signaling controlled by *N*-acyl homoserine lactone. Fig. 2C shows the QS inhibiting activity of both ZN1 and ZN2 at their sub-MIC concentration by interfering with the production of different virulence factors in *P. aeruginosa*. At a concentration of 25–200 μg mL^{-1}, ZN1 demonstrated a dose-dependent decrease in the elastase (35%–74%), total protease (17%–58%) and pyocyanin (25%–67%) production, whereas ZN2 showed more efficacy than ZN1 at the same concentration. Microscopic analysis of the treated biofilm showed a significant decrease in the micro-colonies of the biofilm. The light microscopy result was further confirmed by confocal laser scanning microscopy (CLSM), which showed reduced biofilm biomass after the treatment with 200 μg mL^{-1} ZN1 concentration. This study highlighted the QS inhibiting activity of ZN, which further reduced the production of different virulence factors, and thus controlled the formation of biofilm. Tian *et al.*[98] fabricated chitosan and polyethylene glycol (PEG)-coated Fe_3O_4 nanoparticles to load an antibiotic gentamicin, which showed a strong antibiofilm efficacy at a concentration of 500 μg mL^{-1} against the *S. aureus* biofilm. Dwivedi *et al.*[95] observed that ZnO-NPs synthesized by a soft chemical/solution process were able to eradicate the biofilm and kill *P. aeruginosa* by generating intracellular ROS, which further affected the bacterial DNA and membrane. The low-resolution TEM image of ZnO-NPs demonstrated the smooth spherical morphology with the dimension of the NPs in the scale range of 10–15 nm. The TEM image of the NPs demonstrates the lattice fringes, separated by

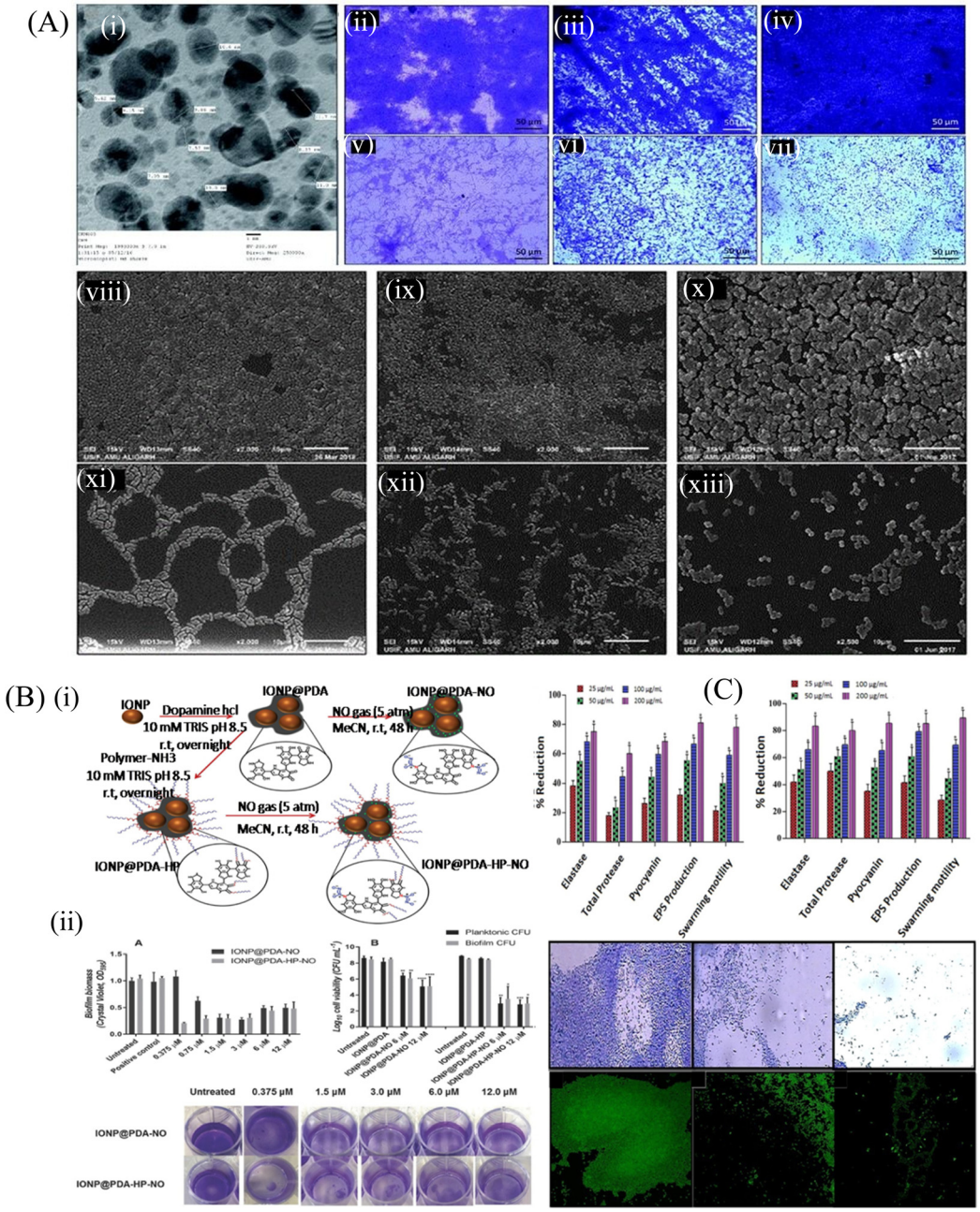

Fig. 2 (A) (i) TEM of TiO_2 NPs recorded at 250 000 magnifications and 200 kV. Light microscopic images showing the effect of TiO_2 NPs on the biofilm development of test bacteria, (ii) control *E. coli* ATCC 25922, (iii) control *P. aeruginosa* PAO1, (iv) control *S. aureus* MTCC 3160, (v) *E. coli* ATCC 25922 treated with 64 mg mL^{-1} TiO_2 NPs, (vi) *P. aeruginosa* PAO1 treated with 64 mg mL^{-1} TiO_2 NPs, (vii) *S. aureus* MTCC 3160 treated with 64 mg mL^{-1} TiO_2 NPs. SEM images showing the effect of TiO_2 NPs on the biofilm development of test bacteria, (viii) control *E. coli* ATCC 25922, (ix) control *P. aeruginosa* PAO1, (x) control *S. aureus* MTCC 3160, (xi) *E. coli* ATCC 25922 treated with 64 mg mL^{-1} TiO_2 NPs, (xii) *P. aeruginosa* PAO1 treated with 64 mg mL^{-1} TiO_2 NPs, (xiii) *S. aureus* MTCC 3160 treated with 64 mg mL^{-1} TiO_2 NPs. All images were captured at 2500 magnification. (B) (i) Schematic illustration of the synthesis of the polydopamine-coated iron oxide nanoparticles (IONP@PDA) and the subsequent reaction with nitric oxide (NO), forming *N*-diazeniumdiolates (NONOates)-functionalized IONP@PDA (IONP@PDA-NO). Another route of synthesis involves the reaction of IONP@PDA with P(OEGMA)-*b*-P(ABA) by the Michael addition reaction, forming P(OEGMA)-functionalized IONP@PDA, IONP@PDAHP. NO was conjugated onto the IONP@PDA-HP to form NONOate-functionalized IONP@PDA-HP, hereby denoted as IONP@PDA-HP-NO, (ii) antibacterial activity of NO-functionalized nanoparticles on *P. aeruginosa*. Bacterial biofilms were grown in multiwell plates for 6.5 h in the absence of any treatment before being treated for a further 30 min with IONP@PDA-NO and IONP@PDA-HP-NO based on various concentrations of NO. The biofilm biomass was analyzed by crystal violet staining. Error bars represent standard error ($n \geq 2$). (B) Effect of the NO-functionalized nanoparticles on *P. aeruginosa* viability after the release of NO. *P. aeruginosa* biofilms were grown in multiwell plates for 6.5 h in the absence of any treatments before being treated for further 30 min in the presence of the nanoparticles at 6 and 12 × 10^{-6} of NO. CFU analysis was used to determine the planktonic and biofilm viability. Error bars represent standard error ($n \geq 2$). Asterisk indicate statistically significance difference of NO-loaded nanoparticles *versus* non-NO-loaded nanoparticles (*, $P < 0.1$; **, $P < 0.01$; ***, $P < 0.001$; ****, $P < 0.0001$). Stained biofilms treated with the indicated concentrations of NO. (C) QS-regulated virulence traits of PAO1: effects of sub-MICs of (i) ZN1 and (ii) ZN2 on inhibition of the QS-regulated virulence factor. Data are expressed as mean % reduction ± SD. Antibiofilm activity of ZNs: images of *P. aeruginosa* biofilm, (iii–v) crystal violet staining under a light microscope. Acridine orange staining under a CLSM, (vi) control, untreated, (vii) 200 μg mL^{-1} of ZN1, and (viii) 200 μg mL^{-1} of ZN2. (A) Reprinted with permission from ref. 93. (B) Adapted with permission from ref. 96. (C) Reprinted with permission from ref. 97.

0.265 nm, and this was similar to the lattice constant of the wurtzite ZnO phase.

4.1.3. Dichalcogenide nanomaterials. Dichalcogenides are a unique class of nanomaterials that have potential applications as antibacterial, antibiofouling, as well as in drug delivery. They kill bacteria by physical disruption, damaging the cell membrane and increasing the membrane permeability through oxidative stress generation. Due to the large surface area and small size, dichalcogenides carry large amounts of drugs and effectively deliver them through the biofilm matrix.[99] Boron nitride (BN) and molybdenum disulfide (MoS_2) are two dichalcogenide nanomaterials that have been explored as antibacterial and antibiofouling agents to prevent the biofilm formation.[100] More often, they are utilized to disrupt the mature biofilm. BN has a honeycomb like structure analogous to graphene. They possess excellent hardness, good chemical inertness, oxidation resistance, thermal conductivity and stability. BN shows biofilm inhibition and bactericidal activity due to their unique properties. BN directly interacts with the bacterial cells, which causes cell damage and leads to cell death. In one study, a BN nanoflakes-embedded low density polyethylene (LDPE) polymer was formulated to eradicate the biofilm of *P. aeruginosa* and *S. aureus*.[101] The BN nanoflakes in this nanocomposite directly interacted with the bacterial cells, and killed the cells through physical disruption of the cell membrane. SEM images of the treated biofilms of *S. aureus* and *E. coli* showed a significant reduction at a concentration of 15% to 20% BN-LDPE nanocomposite compared to the LDPE-treated biofilm (Fig. 3A). MoS_2 is another 2D nanomaterial and forms a sandwich-like structure (S–Mo–S). MoS_2 nanosheets are capable of producing ROS, causing oxidative damage to the cell and leading to cell death.[102] Zalneravicius *et al.*[103] synthesized flower-like sulfur-enriched, hydrophilic MoS_2 nano/microparticles, which were coated with titanium to form a MoS_2/Ti nanocomposite and finally coated with palladium nanoparticles to fabricate the Pd@MoS_2/Ti nanocomposite. Although MoS_2-based compounds are effectual against both Gram-positive and Gram-negative ESKAPE pathogens, the efficacy of Pd@MoS_2/Ti was more prominent on *P. aeruginosa* and the cell viability after treatment for 24 h decreased by 83%, as mentioned in Fig. 3B. Moreover, MoS_2 shows a formidable capability in drug delivery owing to its high surface area. A tetracycline hydrochloride-loaded chitosan-functionalized MoS_2 nanosheet was developed by Zhang *et al.*,[104] where the synergistic effect of both the tetracycline and MoS_2 nanosheet helped to overcome the barrier of the biofilm and kill the bacteria within it. Chitosan reduces the toxicity of the MoS_2 nanosheets. Antibiotics were easily incorporated and delivered to the target site due to the large surface area and hydrophilicity of the MoS_2 nanosheets. As shown in Fig. 3C, the nanosheet attaches to the biofilm structure, leading to the release of the antibiotics and finally disrupting the bacterial biofilms.

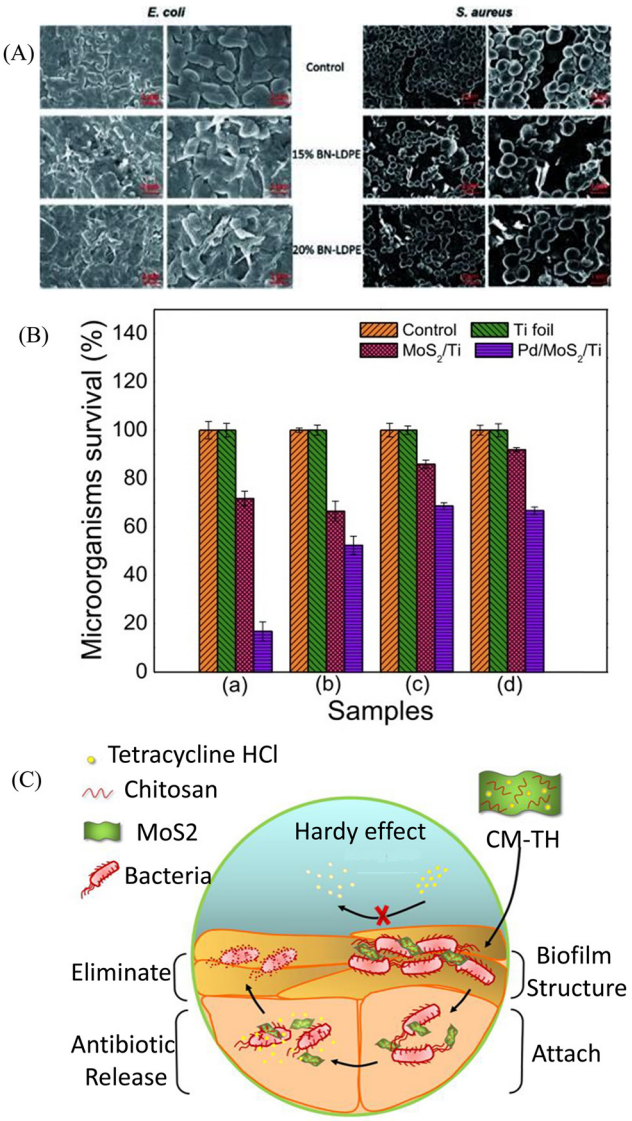

Fig. 3 (A) Representative SEM images of *E. coli* and *S. aureus*. *E. coli* and *S. aureus* were grown for 24 h on LDPE (control) and LDPE composites with 15% and 20% of BN–LDPE composites, and grown bacterial cells were fixed and dehydrated before SEM imaging. (B) MoS_2/Ti and Pd@MoS_2/Ti coatings incubated in liquid nutrient broth and sabouraud media in the presence of *P. aeruginosa* (a), *M. luteus* (b), *C. parapsilosis* (c) and *C. krusei* (d) microorganisms. (C) Scheme of the CM-TH for anti-biofilm applications. Histogram obtained from quantitative analysis. (A) Reprinted with permission from ref. 101. (B) Adapted with permission from ref. 103. (C) Reprinted with permission from ref. 104.

4.2. Carbon-based nanomaterials

Carbon-based nanomaterials are formed from the carbon material with a variety of nanostructures including carbon dots, carbon quantum dots, carbon nanotubes (CNT) and 2D nanomaterials, such as graphene oxide (GO), reduced graphene oxide (rGO) and others. Carbon-based nanostructures have been evaluated as an antibiofilm agent owing to their strong physicochemical and mechanical properties involving physical and chemical damage, including cell membrane damage, metabolic inactivation and ROS-mediated oxidative damage to the bacterial cells.[105]

4.2.1. Carbon dots and carbon quantum dots. Carbon dots (C-dot) have attracted huge interest in biomedical research due

to its good biocompatibility, photostability, low toxicity, great water dispersibility, electron mobility and easy surface modification.[106] They possess various functional groups on their surface, which can conjugate with different drugs and ligands for targeted drug delivery into the biofilm. Li *et al.*[107] demonstrated a pH-responsive antibiofilm nanosystem fabricated by the self-assembly of anionic carboxyl groups of poly(ethylene glycol-COOH-polyethylenimine-2,3-dimethylmaleic anhydride (PPD) with the cationic amines on the surface of C-dots extracted from the calcined L-lysine powder (CDLys) to form the PPD@CDLys nanocomposite. PPD@CDLys penetrates the biofilm structure and becomes positively charged through hydrolysis, leading to the disintegration of the nanosystem. The positively charged PPD subsequently kills the bacteria inside the biofilm through surface attachment. CDLys leads to ROS generation across the entire biofilm of *S. aureus*, disrupts the EPS and ultimately kills the bacterial cells. This entire nanosystem provides dual functionalization against the *S. aureus* biofilm (Fig. 4A). Apart from that, C-dots are also used for imaging purposes. Ritenberg *et al.*[108] fabricated amphiphilic fluorescent carbon dots (C-dot) for imaging purposes of an extrapolymeric substance scaffold of the *P. aeruginosa* biofilm. Due to the small size and linked hydrocarbon chain, C-dot easily penetrated the EPS of *P. aeruginosa*, which helped to visualize the EPS architecture, growth process and the effect of QS inhibitors.

Carbon quantum dots (CQDs) have physicochemical properties similar to those of C-dots, and are used as a great antibiofouling and antibacterial agent. Their small size helps them to easily pass through the biofilm matrix and eradicate the persister cells inside the biofilm. They can be easily formulated by chemical ablation, electrochemical carbonization, microwave irradiation and hydrothermal treatment.[109] Wang *et al.*[110] used bis-quaternary ammonium salt as a carbon and nitrogen source to synthesize nitrogen-doped carbon quantum dots (N-CQDs) nanobiotics (Fig. 4B). The image also demonstrated that the high doses of antibiotics like penicillin and gentamicin (100 × MIC) at different time intervals showed no inhibition of the biofilm even after 4 h of treatment. In contrast, N-CQDs completely eradicated the persister cells of the biofilms in 45 min at a concentration of 8 × MIC. It was also

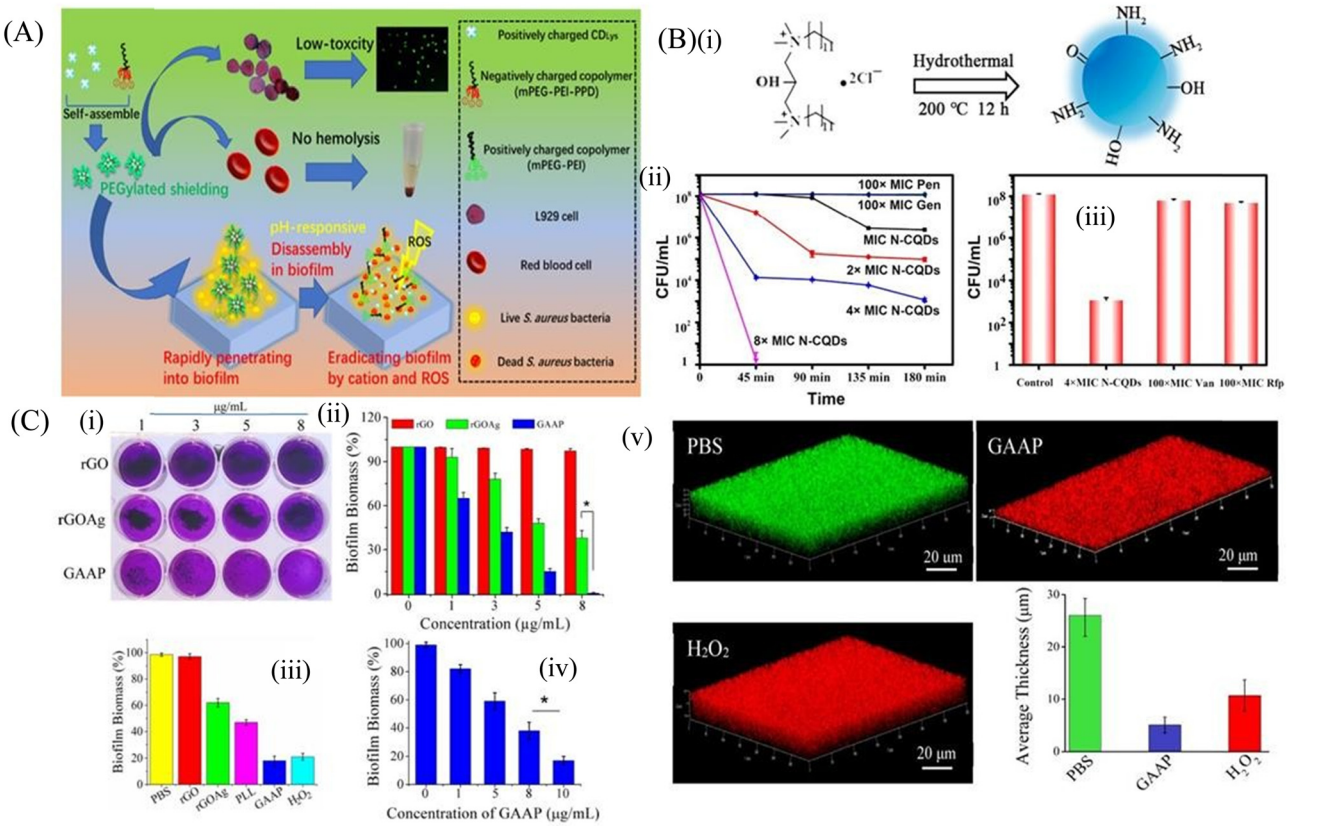

Fig. 4 (A) Schematic representation of carbon dots. (B) (i) Synthesis route of N-CQDS, (ii) N-CQDs, Pen, and Gen were used to fight against persisters. Stationary-phase MRSA cells were treated with different concentrations of N-CQDs (MIC, 2 × MIC, 4 × MIC, and 8 × MIC) and 100 × MIC conventional antibiotics, (iii) Viability of stationary-phase MRSA cells treated with the indicated concentrations of each material for 3 h. The error bars indicate means ± SD (n = 3). (C) Crystal violet assay (i) to measure biofilm formation on rGO, rGOAg, and GAAP after incubation of *S. aureus* for 120 h. (ii) Concentration-dependent biofilm inhibition activity of rGO, rGOAg, and GAAP against *S. aureus*, (iii) activity of rGO, rGOAg, PLL, and GAAP measured by crystal violet staining, (iv) concentration-dependent biofilm disruption by GAAP. (v) Confocal microscopic images of the *S. aureus* biofilm treated with PBS (pH 7.2), GAAP (10 μg mL^{-1}), and H_2O_2 (100 mM). Scale bar, 20 μm. The biofilm was grown for 72 h and treated with GAAP for 5 h at 37 °C; H_2O_2 was used as a positive control and PBS was used as a negative control. (A) Reprinted with permission from ref. 107. (B) Reprinted with permission from ref. 110. (C) Reprinted with permission from ref. 119.

shown that at 4 × MIC of N-CQDs, 90% of the persister cell population was destroyed. On the other hand, 100 × MIC of vancomycin and rifampin were able to eradicate only a small amount of the persister cells of biofilm. This N-CQDs nanosystem also showed strong *in vitro* antibacterial and antibiofilm activity against both MRSA and ampicillin-resistant *E. coli* bacteria without exhibiting any resistance. In addition, it restricted the biofilm formation and disrupted the matured biofilm, and finally accelerated the wound healing cascade when applied on infected wounds. The positively charged N-CQDs attached to the negatively charged bacterial membrane by electrostatic interaction. This led to the membrane damage and increased cellular permeability, which accelerated the insertion of N-CQDs into the cell and finally damaged the DNA through intracellular ROS production. The N-CQDs nanosystem also inhibited the intracellular metabolic pathways of MRSA. Peili *et al.*[111] synthesized a series of CQD_{Gents} from gentamicin sulfate by direct calcinations. The CQDs exhibited antibacterial efficacy as compared to the individual antibiotics. Consequently, the efficacy of these CQDs on the fully matured *S. aureus* biofilm was assessed. The biofilm disrupting capacity of CQDs at 80 μg mL^{-1} was more than 99% as compared to individual antibiotics, which could only disrupt the biofilm by 10%.

4.2.2. Carbon nanotubes. The antimicrobial efficacy of CNTs is mainly due to their electronic structure. They inhibit bacterial adhesion to the substratum because of their mobility, create an unstable substratum for the bacteria and thus inhibit biofilm formation.[112] The vertically aligned arrays of the nanotube are also smaller than the bacteria, which prevent them from entering between the nanotubes.[113] They cause mechanical damage to the cell wall of the bacteria and lead to the efflux of the cellular content of bacteria. Their unique properties like small size, length, and surface chemistry are attributed to their antibacterial property.[114] Treatment of periprosthetic joint infection (PJI) after orthopedic implant surgeries is very difficult due to the formation of bacterial biofilm specifically caused by MRSA. To address this problem, Morco *et al.*[115] discovered carbon-infiltrated carbon nanotube (CICNT) surfaces with a nanopillar structure similar to those of the antibacterial dragonfly and cicada wings. The fabricated CICNT nanostructure facilitated osseointegration, and prevented colonization of MRSA and inhibited MRSA biofilm formation.

4.2.3. Graphene oxide and reduced graphene oxide. Graphene based nanomaterials like GO and rGO are advantageous in biofilm related infections. GO is a 2D carbon nanostructure with a large number of reactive groups like hydroxyl, epoxy, carbonyl, and carboxyl groups on their surface, which can strongly interact with the bacterial surface to show antibacterial activity. Chemical or thermal reduction of GO results in the formation of rGO. Sharp edges of the GO sheet act like nanoknives, which cause cell membrane damage. Membrane stress, leakage of intracellular content, oxidative stress and electron transfer are different modes of action by which GO and rGO show bactericidal effects, which further inhibits biofilm formation and eradication of mature biofilms.[116] Dai *et al.*[117] modified GO nanosheets with tobramycin and copper sulfide nanoparticles as a NIR activated nanosystem for the proper attachment with the bacterial cells and to accelerate the light utilization efficiency of GO. This nanosystem disrupted *P. aeruginosa* and *S. aureus* biofilms under NIR irradiation, and selectively discarded bacterial infection over mammalian cells. According to Yuan *et al.*,[118] nisin, an antimicrobial peptide, conjugated GO selectively to disrupt the biofilm of *S. aureus*. Parandhaman *et al.*[119] developed a novel nanocomposite with graphene, silver and PLL, termed as GAAP (Fig. 4C). Crystal violet staining showed a thick biomass of *S. aureus* biofilm in the case of the rGO-treated sample. However, at a concentration of 8 μg mL^{-1}, rGOAg and GAAP inhibited the biofilm formation. Phosphate buffer saline (PBS) and the rGO-treated biofilm showed a thick biofilm biomass, whereas rGOAg, PLL, GAPP and H_2O_2 treatment decreased the biofilm biomass to 62%, 48%, 17% and 21%, respectively. This result showed that GAPP alone was capable of reducing the biofilm biomass compared to rGOAg and PLL. Then, the dose-dependent effect of GAPP on the biofilm disruption was analyzed, where 80% reduction of the biofilm was observed after the treatment with 10 μg mL^{-1} GAPP. It was due to the conjugation of PLL, which accelerated the antibacterial efficacy of the nanocomposite, and hence target specificity against the biofilm. Upon contact with the anionic bacterial membrane, this cationic conjugate depolarized the bacterial membrane and caused membrane damage. The intracellular ROS generation led to the physical damage of the cell membrane. A quantitative analysis of the biofilm thickness was done where 23.2 μm, 4 μm and 7 μm were observed in the case of PBS, GAAP and H_2O_2, respectively. A series of nanobiocomposite scaffolds were developed by Choudhary *et al.*,[120] where graphene silver-polycationic-peptide (GAP) was incorporated into the chitosan (Cs). Within ten differently synthesized scaffolds, Cs-GAP 100 with 100 μg mL^{-1} GAP concentration exhibited excellent mechanical strength. Cs-GAP 100 also showed poor degradation properties with a large surface area. The hydrophilic nature of the peptide provided enhanced fluid and blood absorption capacity. Cs-GAP also showed good antimicrobial properties against *S. aureus*, which makes it a potential nanocomposite for hemorrhage control and wound healing application.

4.3. Lipid-based nanomaterials

Lipid-based nanoparticles like liposome, solid lipid nanoparticle and nanostructured lipid carrier also draw great attention in the biomedical field. Their versatility, biocompatibility, solubility and high drug loading capacity makes them potential biofilm-targeted nanosystems.

4.3.1. Liposome. Biofilm-related infections in surgical wounds are difficult to treat because most of the antibiotics cannot reach the deeper tissues and lead to systemic pathogenesis. To overcome this limitation, liposomal formulation has been explored to treat the biofilm-related bacterial infections as it directly penetrates into the necrotic tissue and eradicates both intra and extracellular bacteria. Liposomes are bilayer structures ranging from 50 nm to 1000 nm. Liposomes can be

uni, oligo and multi-lamellar depending on the presence of the bilayer.[121] They can be further classified as cationic, anionic, zwitterionic and fusogenic liposomes. Liposomal formulation is often used to deliver poorly water-soluble drugs into the biofilm matrix. Liposomal formulation can also protect the drug from enzymatic degradation and inactivation by the low pH of the microenvironment of the matrix. Different liposomal formulations are prepared to deliver antibiotics, which inhibit biofilm formation, as well as disrupt the preformed biofilm.[122] The size and surface charge of the liposome also play a significant role in the delivery of the antibiotics into the biofilm matrix. Reduction of the size enables the liposome to effortlessly penetrate the biofilm matrix, whereas a positive charge provides enhanced interaction with the negative components of the biofilm matrix. To increase the efficacy of the liposomal formulation, the size and surface charge of the liposome were further tuned by both Hou *et al.*[123] and Dong *et al.*[124] Hou *et al.*[123] reported a lysozyme-stabilized gentamicin-loaded liposomal formulation to impart the positive charge to the liposomal formulation. The positively charged liposome interacts with the alginate of the *P. aeruginosa* and *S. aureus* biofilm, and effectively removes the biofilm of both Gram positive and Gram-negative bacteria compared to gentamicin and lysozyme alone. The size and zeta potential of liposomal gentamicin was 99 nm and −54.5 mV, respectively. The zeta potential of lysozyme associated with liposomal gentamicin became 17.5 mV, which was a clear indication that the positively charged lysozyme was associated with the negatively charged liposome due to the change in the zeta potential value. This lysozyme-associated liposomal gentamicin significantly reduced the biofilm biomass and viable cell count in both *S. aureus* and *P. aeruginosa*, whereas gentamicin or lysozyme alone did not show any significant reduction. Fluorescence microscopy imaging further confirmed the potential antibiofilm effect of lysozyme-associated liposomal gentamicin (Fig. 5A). Dong *et al.*[124] prepared cationic liposomes with reduced size, which demonstrated greater penetration properties, along with strong anti-biofilm activity against *P. aeruginosa* and *S. aureus* biofilm. They prepared both cationic and anionic liposomes to compare their properties, such as the size and charge distribution within the biofilm. This study revealed that the unilamellar vesicles were more efficient in penetrating the *P. aeruginosa* and *S. aureus* biofilms than the multilamellar vesicles bearing the same charge as the unilamellar vesicles. Apart from this, vancomycin-encapsulated liposome was further functionalized with a 27 kDa endopeptidase lysostaphin to eradicate MRSA. This peptide specifically binds to the peptidoglycan of *S. aureus.* The α-toxin of MRSA was responsible for the release of vancomycin from the liposome, which gave a synergistic effect,where lysostaphin and vancomycin both accelerated the killing procedure of MRSA.[128] Stimuli responsiveness is another way to make the liposome more effective and target specific, while eliminating toxic effects. Zhao *et al.*[125] developed a thermosensitive liposome (TSL) consisting of distearoylphosphotidylcholine and betainylate cholesterol, which could encapsulate antibiotic and cyanine dye (cypate). Due to the presence of cypate dye within the liposome, TSL showed a strong absorption in the NIR region with a maximum absorption peak at 782 nm. Under NIR laser irradiation, cypate dye converted the absorbed photon into heat, which was responsible for the temperature change of the liposomes. The NIR light could increase the temperature from 27.1 to 75.5 °C within 5 min at a minimum concentration of 31.3 μg mL^{-1} of liposomal formulation. This indicated that the laser energy was absorbed by cypate and effectively converted to thermal energy. This liposome could effectively enter the biofilm, after which the drug was released in a thermo-sensitive manner, leading to the disruption of the biofilm of *P. aeruginosa* and accelerating the wound healing.

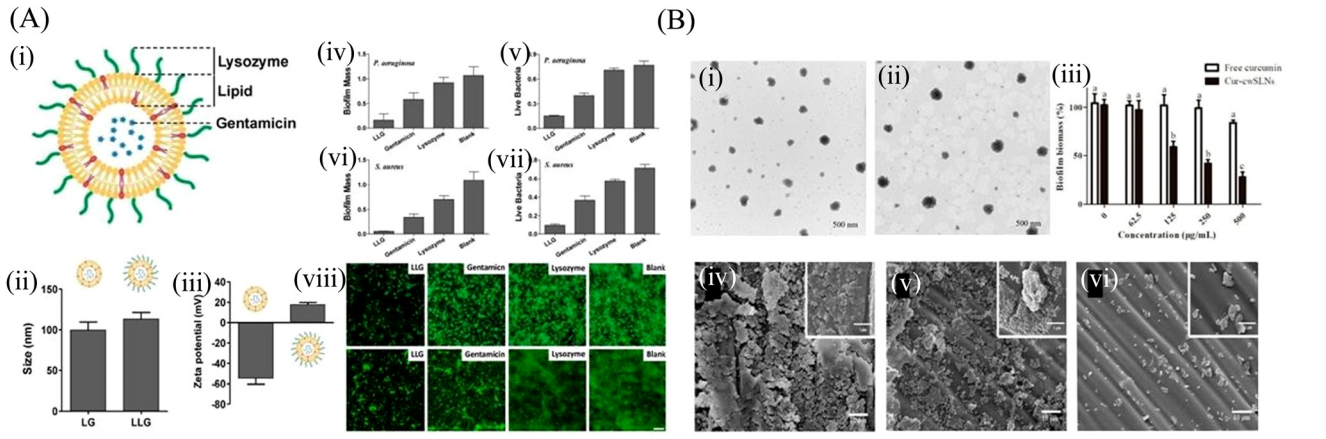

Fig. 5 (A) (i) Schematic structure of lysozyme-associated liposomal gentamicin (LLG), (ii) hydrodynamic size, and (iii) surface zeta potential of liposome (without Lysozyme) and LLG, Crystal violet assay and 3-(4,5-dimethyl-thiazol-2-yl)-2,5-diphenyltetrazolium bromide (MTT) assay to assess the antibiofilm activity of LLG against *P. aeruginosa* biofilm (iv and v) and *S. aureus* (vi and vii). Fluorescence microscopy of *P. aeruginosa* (viii) and *S. aureus* (ix) biofilms. Biofilms incubated with tryptic soy broth (TSB) are used as the control. Scale bars were 10 μm. (B) The TEM of the SLNs (i) cwSLN, (ii) Cur-cwSLN, (iii) the cytotoxicity of cwSLNs and Cur-cwSLNs in 24 h. Data are presented as the mean ± SD, n = 3, (iv) SEM image of *S. aureus* biofilms, (v and vi) SEM image of inhibitory effects of pure curcumin and Cur-cwSLNs against biofilms produced by *S. aureus*, respectively. (A) Reprinted with permission from ref. 123. (B) Adapted with permission from ref. 131.

4.3.2. Solid lipid nanoparticles and nanostructured lipid carrier. Solid lipid nanoparticle (SLN) is an alternative carrier system of different colloidal carriers. It is a type of lipid nanoparticle, where the liquid lipid part is replaced by a solid lipid like fatty acids, triglycerides and/or steroids.[126] On the other hand, nanostructured lipid carriers (NLC) are the next generation SLN with improved loading capacity, stability and long storage life. Both SLN and NLC are composed of lipids, which are equivalent to those in the skin and sebum. It makes them more biocompatible to deliver antimicrobial agents through the skin tissues to target sites, and eradicate the biofilm-related infections.[127] To combat biofilm-related pulmonary infections caused by *P. aeruginosa* and *S. aureus*, ofloxacin-loaded SLN was formulated, which showed selectivity, sustained drug release at the target site and enhanced potency. This nanocomposite shows a 3-fold decrease in MIC compared to free antibiotics.[128] In another study, oxacillin-loaded NLC was formulated to increase the efficacy of oxacillin against MRSA.[129] Oxacillin-loaded NLC showed synergistic activity against MRSA, where the bactericidal concentration of oxacillin against MRSA was reduced from 250 μg mL^{-1} to 62.5 μg mL^{-1}. This study revealed that this combination is more effective in disintegrating the biofilm architecture than the individual treatment of oxacillin and NLC. Furthermore, to enhance their stability and effectiveness against the biofilm, different surface modifications were attempted. A chitosan and deoxyribonuclease (DNase)-modified SLN loaded anacardic acid (Ana) has been reported, where chitosan provided stability, integrity of the SLN and DNase degraded the eDNA of biofilm.[130] Biofilm of *S. aureus* decreased in a dose-dependent manner upon treatment with Ana-SLNs-CH-DNase. Ana-SLNs-CH-Dnase exhibited detachment of the biofilm up to 36.40 ± 2.38% at a concentration of 0.097 μg mL^{-1}. Therefore, it is suggested that the positive charge of the chitosan interacted with the negatively charged component of the biofilm matrix, and thus helped it adhere to the SLN with the biofilm. Recently, wax SLN showed increased attraction compared to glyceride-SLN because of their uniform particle size distribution and physical stability. Curcumin (cur) has well-documented antimicrobial properties. However, its application is limited due to its poor solubility. To overcome this limitation, wax-based SLN was formulated by Luan *et al.*[131] using Chinese white wax solid lipid nanoparticle (CW SLN), which was loaded with cur. Cur-loaded Chinese white wax SLN remarkably interferes with the formation of the biofilm, which led to biofilm inhibition. The TEM image suggests that the Cur-CW-SLN size was larger than that of CW-SLN, which proved that cur was efficiently loaded into CW-SLN (Fig. 5B). A concentration of 125 μg mL^{-1} Cur-CW-SLN inhibited the formation of the biofilm, whereas free cur was unable to show any significant effect in the inhibition of the *S. aureus* biofilm even at a concentration of 500 μg mL^{-1}. The SEM micrograph revealed that Cur-CW-SLN was more effective in the inhibition of the biofilm than free cur.

4.4. Polymeric nanomaterials

Polymeric nanomaterials range from 10 to 1000 nm in size. There are different kinds of polymeric nanomaterials like polymeric shells or polymeric matrices. They are extensively used to deliver antimicrobial agents due to their high solubility index.[132] They can be modified easily by different antimicrobial agents or peptides to achieve the desirable target-oriented removal of biofilms.

4.4.1. Polymeric micelles. Micelles are self-assembly amphiphilic copolymers having both hydrophilic (polar region) and hydrophobic (non-polar) regions. The hydrophilic outer core of this nanocarrier can carry water-soluble drug, whereas the hydrophobic inner core is able to deliver poorly water-soluble drugs. These structures have attracted much attention as antibiofouling agents because of their controlled and sustained release of drugs to the target site, providing chemical and physical stability of the encapsulated drug and improving drug bioavailability.[133] Micelles can act either as antibacterial agents or they can be used as delivery systems of antimicrobial agents. It is reported that polypeptide-based micelles are excellent antibacterial and antibiofouling agents. Xi *et al.*[134] synthesized a peptide-based copolymer poly(L-lactide)-*block*-poly(phenylalanine-*stat*-lysine), which was self-assembled into a micelle. These micelles demonstrated antibacterial effect against *S. aureus* and *E. coli*, and damaged the bacterial membrane, leading to the outflow of the cytoplasmic contents. Hisey *et al.*[135] synthesized phosphonium-functionalized block copolymer micelles, where phosphonium cations with different alkyl lengths like tri-*n*-butyl, triethyl and tri-*n*-octyl were conjugated to the terminus of a poly(ethylene oxide)-polycaprolactone block copolymer. Subsequently, phosphonium-functionalized block copolymers having different chain lengths were self-assembled to form micelles and utilized to study the antibacterial efficacy. Among all these polymeric micelles, the tri-*n*-octyl block copolymer micelle showed better bactericidal efficacy against *S. aureus*. However, tri-*n*-butyl demonstrated better efficacy against *E. coli.* Furthermore, the tetracycline was incorporated into this micellar system, which provided an orthogonal mode of action against *S. aureus* and *E. coli*. In another study, Qiao *et al.*[136] prepared polymeric micelles using poly(lactic-*co*-glycolic acid)-*block*-methoxy poly(ethylene glycol) (PLGA-*b*-mPEG) and poly(lactic-*co*-glycolic acid)-*block*-poly(terpyridine)$_5$, to chelate Fe(II) ions required for the formation of *P. aeruginosa* biofilm. Under aerobic conditions, the as-prepared block copolymer micelle reduced the biofilm formation of the PAO1 and ATCC 27853 strain at a concentration of >128 μM. Under anaerobic conditions, this micelle requires a concentration as low as >4 μM to inhibit the PAO1 and ATCC 27853 strain. This reported micelle serves as an excellent antimicrobial agent, which can inhibit the biofilm mass production of *P. aeruginosa* in anaerobic conditions. Park *et al.*[137] used a self-assembled chimeric antimicrobial lipopeptide (DSPE-PEG-HnMc) and an amphiphilic biodegradable polymer (PLGA-PEG) to formulate a chimeric micelle named as HnMc. This chimeric HnMc targeted the plasma membrane of *P. aeruginosa* and effectively killed the bacteria. The HnMc prepared with 2 : 8 ratios of DSPE-PEG-HnMc and PLGA-PEG demonstrated better antibacterial efficacy than the HnMc prepared by 1 : 9 ratios at their critical micelle concentration (CMC). A 90% growth reduction of the

drug-resistant *P. aeruginosa* CCARM 2073 and *S. aureus* CCARM 3078 was observed in the case of HnMc (2 : 8) at a concentration of 0.05 mg mL^{-1}. Moreover, HnMc was able to inhibit biofilm formation of the above pathogens at a concentration of 0.1 mg mL^{-1}, which established it as an excellent peptide-based nanomedicine for the treatment of bacterial infections. The micelle can be modified to make it stimuli-responsive to increase specificity towards the site of infections. Guo *et al.*[138] synthesized the pH-sensitive micelle to target the biofilms, whereas Chen *et al.*[139] formulated a pH/lipase-sensitive micelle to deliver ciprofloxacin to the *P. aeruginosa* biofilm. Guo *et al.*[138] had synthesized three different types of pH sensitive copolymers named PAE–PLA–mPEG (A–L–E), PLA–PAE–mPEG (L–A–E) and PLA–PEG–PAE (L–E–A) composed of poly(β-amino ester) (PAE), poly(lactic-*co*-glycolic acid) (PLA) and polyethylene glycol (PEG), respectively, which were self-assembled in aqueous medium. The pH-sensitive chains that are PLA–PAE–mPEG, PAE–PLA–mPEG and PLA–PEG–PAE were self-assembled into micelles $M_{L–A–E}$, $M_{A–L–E}$ and $M_{L–E–A}$, respectively, where PLA was a hydrophobic core, PEG was a stable shell and PAE presented as pH-sensitive hydrophobic core moieties. They observed that at the triggering pH (pH at which the surface charge becomes reversed, pH_t) on the biofilm surface, both the $M_{L–A–E}$ and $M_{L–E–A}$ were able to regulate the charge switching at the pH of 5.5 and 6.0, respectively (Fig. 6A). It is shown that $M_{L–A–E}$ effectively eradicates the implant-related biofilm infections, which can efficiently remove biofilms from the catheter. Chen *et al.*[139] designed a vancomycin-functionalized micelle encapsulated with ciprofloxacin (CIP). Vancomycin-mediated targeting and pH/lipase-dependent release of CIP from the micelle shows higher survival of *P. aeruginosa*-infected mice. At pH 7.4 and 6.0, 20% release of CIP was observed, while in the presence of lipase enzyme, around 39 to 56% CIP release was found. A single dose of Van-hyd-PECL/Cip micelles reduced the bacterial load in lung tissues by around 3.1-log_{10} fold in comparison to the free Van-CIP. These micelles provided a workable infection microenvironment-responsive strategy to combat bacteria.

4.4.2. Dendrimers. Dendrimers are a group of highly branched spheroid polymeric substances used as a carrier for drug delivery and also applied as nanodrugs.[140] Dendrimers can be made to be either cationic, anionic or amphiphilic. Among them, cationic or amphiphilic dendrimers disrupt the lipid bilayer structure of the bacterial cell membrane and increase the cell membrane permeability, which leads to cell death. The number of active groups and the branching of the dendrimer influence their role as antimicrobial agents. Poly(propylene imine) dendrimers demonstrate good antimicrobial activity against *S. aureus*.[141] The surface of (propylene imine) dendrimers was further modified with different concentrations of maltose. It was observed that maltose at a concentration of 25% showed good selectivity against *S. aureus* without damaging the host cells. Antimicrobial dendrimeric peptides (AMDP) are a new class of antimicrobial and anti-biofilm agents. 2D-24 is an antimicrobial dendrimer synthesized by Bahar *et al.*,[142] which eradicated 94.4 ± 1.4 and 93.9 ± 4.2% of PAO1 and PDO300 biofilm cells at a concentration of 30 μm, respectively. Multivalent peptide dendrimers are also reported to attach to the lectin of bacteria and interfere with the bacterial surface attachment. Multivalent fucosyl-peptide dendrimer FD2 specifically bind to the fucose specific lectin LecB and LecA of *P. aeruginosa*, and was shown to cause 30% and 40% inhibition of biofilm formation at a concentration around 50 μM, respectively.[143] (Fig. 6B). LecB protein is no longer able to attach to the surfaces upon binding with the FD2 dendrimer, and thus inhibit the biofilm formation along with disrupting the mature biofilm. Apart from that, the dendrimer can also act as a carrier and deliver the antibacterial agents to the target site. Levofloxacin (LEV)-loaded $MalG_2(SNHMe_2Cl)_4$, a cationic carbosilane dendron, eradicates *S. aureus* biofilm efficiently.[144] To enhance the antibiofouling activity, this dendron was conjugated with a cell-penetrating peptide called gH625, which can enter the biofilm and then disrupt the bacterial membrane bilayer. $MalG_2(SNHMe_2Cl)$ had a maleimide group at the focal point that provided the anti-biofilm property. This study showed that a dendron in combination with peptide and levofloxacin efficiently prevent biofilm formation, and eradicates the established biofilm. Branched water-soluble dendrimers, such as polyamidoamine dendrimers (PAMAM) with high surface area, have also been explored to deliver antibiotics. Different generations of PAMAM with hydroxyl and amine groups are used to increase their solubility in water. PAMAM-NH_2 (generation 2 and 3) and PAMAM-OH (generation 3) dendrimers increase the solubility of poorly water-soluble erythromycin up to 7–8 fold. Moreover, they caused 2- and 4-fold reductions of the MBC value against *S. aureus*, respectively.[145]

4.4.3. Polymersomes. Polymersomes are composed of both hydrophobic and hydrophilic copolymers that self-assemble together, and results in a vesicle-like structure in aqueous solution. Polymersomes have a hollow membrane-like structure composed of hydrophilic inner and outer parts, and the hydrophobic parts remain associated with each other to avoid exposure to the aqueous phase.[146] Polymersomes have a thick membrane, which gives them enhanced stability, rigidity and increased efficiency to encapsulate drugs. The prolonged systemic circulation and release profile of the polymersome renders it more beneficial than the liposomes. The polymersome easily fuses with the cell membrane of the host cell and delivers the antibiotics. Therefore, they are often used for targeted drug delivery to kill the intracellular bacterial pathogens. Periodontitis is caused by plaque biofilms of different bacteria. A dual corona vesicle composed of two block copolymers that is poly(ε-caprolactone)-*block*-poly(lysine-*stat*-phenylalanine) [PCL-*b*-P(Lys-*stat*-Phe)] and poly(ethylene oxide)-*block*-poly(ε-caprolactone)[PEO-*b*-PCL] was fabricated (Fig. 6C) to deliver CIP and remove periodontitis.[147] These block copolymers of the formulated polymersome have their specific role as an antibiofouling agent. This CIP-loaded nanosystem can eradicate the plaque biofilm with a 50% reduction of CIP dosage. This CIP-loaded nanosystem also exhibited excellent efficacy in rat periodontitis, which removes biofilm plaque and reduces inflammation. In another study, Hong *et al.*[148] designed a

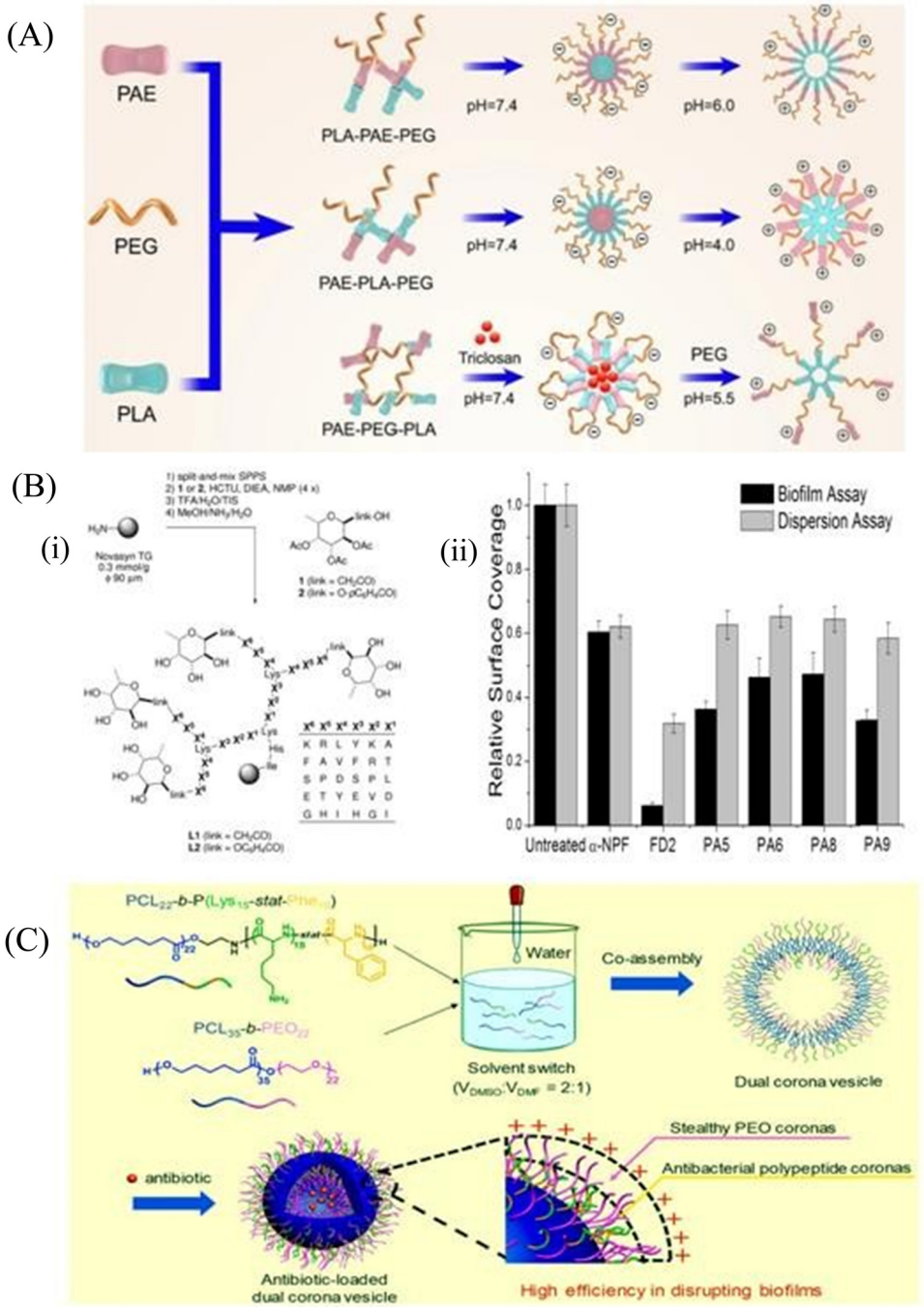

Fig. 6 (A) Elaboration on the architecture of pH-sensitive copolymers with proper pH. (B) (i) Synthesis and structure of the *C*-fucosyl peptide dendrimer libraries, displayed on tentagel resin as solid support. The 'link' between amino acid X6 and the fucose is either an acetyl spacer in the *C*-fucosyl library L1 or phenoxyacyl in the *O*-fucoside library L2, obtained by coupling the corresponding building blocks 1 and 2. The positions X1–X6 display various amino acids according to the table at right (one-letter codes of L-amino acids) as a 'one-bead-one-compound' library obtained by the split-and-mix SPPS protocol, (ii) biofilm assays with *P. aeruginosa* and dendrimers. Biofilm inhibition and dispersion were tested with a-NPF (0.5 mM), dendrimers (0.05 mM), and wild-type strain PAO1. The values are normalized so that growth without any inhibitor is set to 1. A background control (no bacteria) gave reading values similar to the ones shown in the graph for the FD2 biofilm assay (0.05 mM). Mean values of three independent readings ± standard deviation are plotted. (C) PCL22-*b*-P (Lys$_{15}$-*stat*-Phe$_{10}$) and PEO$_{22}$-*b*-PCL$_{35}$ copolymers are co-assembled into a dual corona vesicle that can further encapsulate ciprofloxacin. (A) Reprinted with permission from ref. 138. (B) Reprinted with permission from ref. 143. (C) Reprinted with permission from ref. 147.

penicillin G-entrapped PCL-*b*-P (Lys-*stat*-Phe) polymersome. Furthermore, this polymersome was cross-linked with dibenzaldehyde-functionalized-PEG (DE-PEG) to form hydrogels, which impart two-stage antibacterial activity. The polymersome-hydrogel nanocomposite showed prolonged drug release compared to free polymersome. Furthermore, Walvekar *et al.*[149]

reported hyaluronic acid-oleylamine (HA-OLA) conjugates as an effective drug carrier to treat MRSA infection. The HA-OLA polymersome was prepared by self-assembling process, which carried 26.1–43.12% vancomycin. Sustained drug release up to 72 h from HA-OLA polymersome killed MRSA very efficiently. Gram-negative bacteria are an easy target of boronic acid because boronic acid can react with the *cis*-diols of LPS in the bacterial outer membrane. However, boronic acid binds with LPS of the bacteria through weak interactions. To improve the binding efficacy of boronic acid with LPS, Wang *et al.*[150] used phenylboronic acid and formulated *O*-(bromomethyl) phenyl) boronic acid encapsulated poly((2-*N*,*N*-diethyl)-aminoethyl acrylate) (PDEA) polymersome. This nanosystem can eradicate 99% of the bacteria in the biofilm at a concentration of 64 μg mL^{-1}. The strong covalent bonding between phenylboronic acid and the LPS layer of *E. coli* and the electrostatic interaction between the cationic copolymer and the anionic lipid of the outer membrane led to the cell lysis and eradication of the biofilm.

4.5. Nanoemulsion

Emulsions are thermodynamically stable colloidal dispersions of two immiscible liquids. Emulsions can be macro, micro and nano size droplets depending upon their size. Nanoemulsions are a type of nanosized emulsions consisting of interdispersed hydrophobic and hydrophilic layers forming a nanocarrier system. Nanoemulsions are synthesized by high pressure homogenizer, high sheer stirring, ultrasound generator, and microfluidization.[151] Owing to their small size along with solubilization properties, nanoemulsions can overcome the barrier of the biofilm matrix and deliver the antimicrobial agents to eradicate bacterial biofilms. Prateeksha *et al.*[152] developed a nanoemulsion with the bioactive compounds of *Gaultheria fragrantissima* wall essential oil (EO), *viz.*, eugenol (E-NE) and methyl salicylate (MS-NE) to inhibit the virulence and biofilm growth by *E. coli* O157:H7 (ECOH). COMSTAT analysis (Fig. 7A) demonstrated that the nanoemulsions made up of eugenol and methyl-salicylate prevented biofilm formation, and the substratum coverage and mean thickness were reduced by more than 80%. Nanoemulsion-loaded hydrogel coatings are preferably used to combat *E. coli* infestation on solid surfaces by their antibiofouling strategy. In another study, Ramalingam *et al.*[153] synthesized a nanoemulsion containing EDTA with a mean diameter of 269 nm to show its inhibitory effect on the biofilm formation by *A. baumannii*. The nanoemulsion particularly prevented the adherence of the bacterial cells on the glass surface and restricted biofilm formation. For

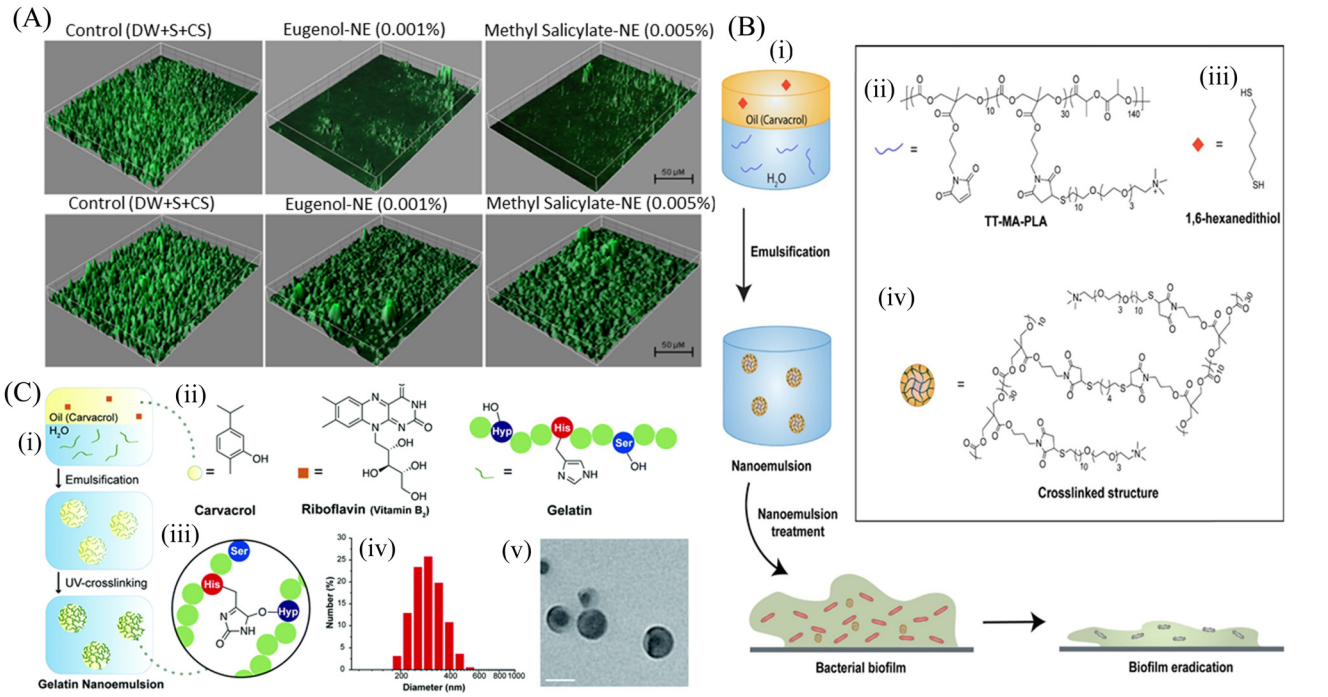

Fig. 7 (A) Anti-biofilm activity of hydrogel coatings containing eugenol-NE and methyl salicylate-NE, eugenol and methyl salicylate against ECOH on glass surfaces, measured by CLSM. The mixture of DW, surfactant (S; Tween 80) and co-surfactant (CS; propylene glycol) in the ratio of 94.7 : 0.2 : 0.1 was used as a solvent control. (B) Schematic representation of the strategy utilized to generate carvacrol-loaded nanoemulsions, (i) resulting nanoemulsions showed improved antimicrobial activity against MDR bacterial biofilms, (ii) chemical structure of TT-MAPLA, (iii) chemical structure of 1,6-hexanedithiol, and (iv) Cross-linked structure of X-NEs. (C) Fabrication and characterization of gelatin nanoemulsions, (i) Riboflavin (UV cross-linking initiator) was dissolved in carvacrol. The oil mixture was then emulsified in an aqueous gelatin solution and cross-linked using long wavelength UV-A light (365 nm) to fabricate gelatin nanoemulsions, (ii) chemical structures of carvacrol, riboflavin, and the functional groups of gelatin participating in the cross-linking reaction, (iii) proposed cross-linked structure of gelatin nanoemulsions, (iv) dynamic light scattering histogram of nanoemulsions in PBS (150 mM), (v) TEM images of nanoemulsions. Scale bar is 100 nm. (A) Reprinted with permission from ref. 152. (B) Adapted with permission from ref. 154. (C) Adapted with permission from ref. 155.

further stabilization of the nanoemulsion, various crosslinked nanoemulsions were prepared. Oz *et al.*[154] synthesized a novel formulation based on a nanoemulsion, which was stabilized by cross-linked PLA (Fig. 7B). This polymer scaffold was highly antibacterial and exhibited strong antibiofilm efficacy against matured *E. coli*, *A. baumannii*, and MRSA biofilm. This stable nanoemulsion was made by the cross-linking of maleimide-functionalized PLA (MA-PLA) with the help of a dithiol crosslinker *via in situ* maleimide-thiol Michael addition. To increase its solubility, a dithiol crosslinker was developed. The nanoemulsion was loaded with carvacrol to disrupt the matured biofilms. Li *et al.*[155] prepared a gelatin photo-crosslinked carvacrol nanoemulsion using a riboflavin photocatalyst. This antimicrobial nanoemulsion exhibited antibiofilm efficacy, and subsequently accelerated the wound healing by eradicating the wound biofilm of *P. aeruginosa* and MRSA (Fig. 7C). In spite of this progress, there are many drawbacks associated, such as poor stability due to the continuous fusion of the droplets, causing their aggregation. In addition, they are non-specific to the bacterial cell membrane.[154] To overcome these limitations, Song *et al.*[156] fabricated an antibacterial and antibiofilm chlorhexidine acetate nanoemulsion (CNE) for MRSA-infected skin burn wounds. CNE mostly targets and damages the cell wall and cell membranes of MRSA, leading to the release of alkaline phosphates, K^+, Mg^{2+}, DNA and protein, causing increased relative electrical conductivity. Hwang *et al.*[157] demonstrated that ananoemulsion formulated with cetylpyridinium chloride (CPC) possessed antibacterial activity against planktonic and biofilm-forming *A. baumannii*. The CPC nanoemulsion helps in killing the planktonic bacterial cells, while the emulsified oil and detergent fractions degrade the biofilm structure. Recently, Das *et al.*[158] developed a novel cationic nanoparticle conjugated oil in a water nanoemulsion to impart positive charges to the nanoemulsion for effective antibacterial and antibiofilm activity against *S. aureus* biofilms. The conjugated formulation penetrated the biofilm matrix and killed the persister cells through electrostatic interaction. In this manner, the matured biofilm was disrupted and new cells were restricted from adhesion, *i.e.*, biofilm inhibition.

5. Antibiofouling mechanism of nanomaterials

The antibiofouling mechanism could be divided into two major activities, as follows: (1) inhibition of biofilm formation and (2) disruption of the existing biofilm (Scheme 5). Surface modification or the use of an agent that can interfere with the cell attachment to the surface can prevent biofilm formation. On the other hand, the preformed biofilm can be eradicated by the destruction of the EPS matrix and killing of the dispersed cells.[159]

5.1. Biofilm inhibition

Biofilm formation occurs in three consecutive stages, as follows: (i) attachment, (ii) colonization and proliferation of bacterial cells, and (3) maturation of the biofilms. Nanoparticles play an important role in the prevention of biofilm formation by inhibiting the initial attachment of planktonic cells on the substratum owing to its strong antibacterial activity. Nanomaterials inhibit bacterial adhesion because of their mobility creating an unstable substratum for the bacteria inhibiting the formation of a biofilm.[112] Nanoparticles can reduce adhesion, maturation and proliferation of the biofilm by the formation of ROS, such as H_2O_2, hydroxyl radical (OH^-) and superoxide ions (O^{2-}). Nanomaterials interact with the

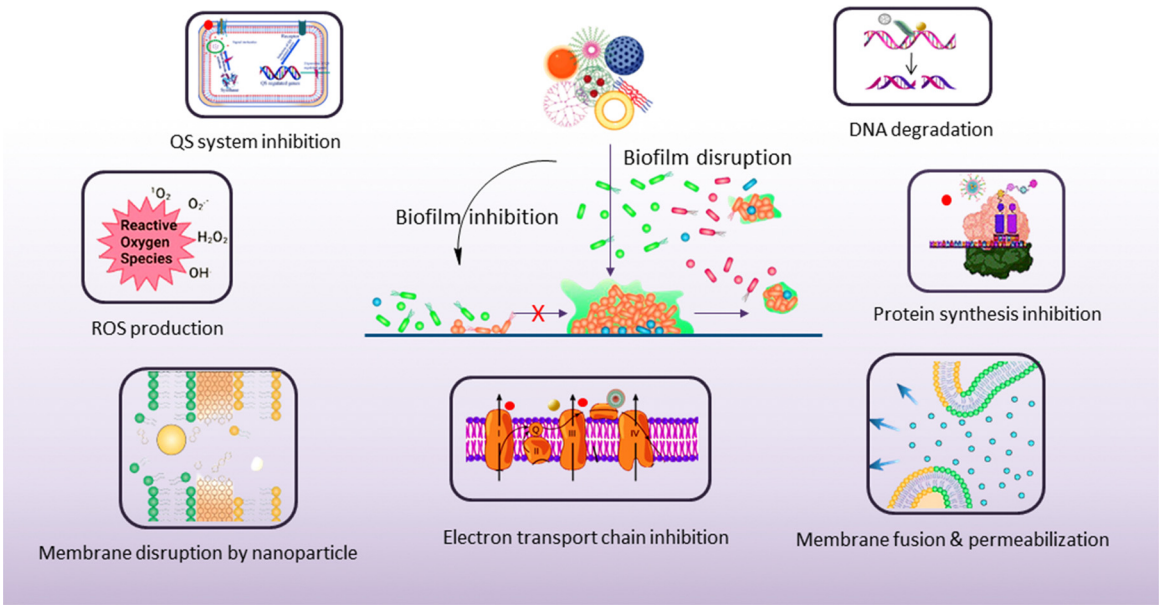

Scheme 5 Biofilm inhibition and disruption mechanism of nanomaterials.

bacterial cells and exhibit antibacterial activity through multiple pathways, which include membrane depolarization, ROS generation, inhibition of respiratory chain enzymes, damage of the intracellular components, inhibition of DNA replication and protein synthesis.[158,160] Oxidative stress is an important factor mediated by metal nanoparticles that causes cytotoxicity and genotoxicity to the bacterial cells.[161] Oxidative stress-related damage is of two types: ROS-dependent and ROS independent. The ROS-dependent pathway involves the overproduction of OH^-, O_2^- and H_2O_2 to damage the cell membrane, destroy proteins, inhibit DNA replication and causes the leakage of intracellular components of the bacterial cells. Metal nanoparticles like AgNPs, AuNPs, and CuNPs bind with the bacterial cell membrane, resulting in the loss of cellular integrity, membrane damage, alteration of membrane permeability and exudation of cytoplasmic contents.[80,90] In addition, ROS generation takes place, which leads to oxidative damage of the cellular components. Metal ions leached out from nanoparticles also contribute to antibacterial activity through the oligodynamic effect by destroying the proteins of the bacterial cell wall. Metal ions binding with the cell wall cause inhibition of respiratory chain dehydrogenase, uncoupling of oxidative phosphorylation, and metabolic arrest in the cells.[162] Nanoparticles like AuNPs, AgNPs, and CuNPs also show peroxidase-like activities by converting H_2O_2 into toxic OH radicals to kill bacteria.[163–165] The size, shape and surface properties of the nanoparticles play a pivotal role in the inhibition of biofilm formation. Smaller size nanoparticles show high antibacterial activity due to the high surface area-to-mass ratio and large interaction with the bacterial surface. It results in the disintegration of the bacterial cell wall, alteration of the membrane potential, destabilization of the outer membrane and leakage of the cytoplasmic contents.[166,167] The shape of the nanoparticles also plays a significant role in the contact killing of bacterial cells. Sharp and pointed nanoparticles rupture the cell membrane of bacteria, leading to the leakage of cytoplasmic contents. Surface functionalization of the nanoparticle is another important factor, which enables multiple interactions with the bacterial cells and enhances the biofilm inhibition properties of nanomaterials. Surface modification of nanoparticles with different ligands and chemical groups, such as antimicrobial peptides, different polymers, and aptamers, strengthens interactions such as hydrophobic, electrostatic and van der Waals interactions between bacteria and nanoparticles. Cationic nanoparticles bearing a net positive charge interact with the negatively charged bacterial cell surface, leading to enhanced uptake of nanoparticles into the cells.[168] This causes surface charge alteration, depolarization of the membrane potential, intracellular ROS generation and membrane pore formation.

Nanomaterials can also be modified in such a way that it can interfere with the intracellular signaling pathways and disturb the cellular homeostasis. These disruptions include alteration in gene expression, DNA damage and protein synthesis. AuNPs functionalized with 4,6-diamino-2-pyrimidinethiol (DAPT) are able to inhibit the synthesis of bacterial tRNA.[169] Au-DAPT binds to the genetic material, ribosomes, and inhibits protein synthesis of MDR strains of *E. coli* and *P. aeruginosa*. Au-DAPT also chelates Mg^{2+} ions, which results in destabilization of the bacterial cell membrane, followed by cell death. Nanoparticles can also act as carriers for loading antimicrobial drugs to increase the effectiveness, biocompatibility and bioavailability of antibiotics.[99,121] Antibiotics, drugs and different therapeutics can be easily delivered either by encapsulating or conjugating with the nanomaterials.[127,139] These nanomaterials protect them from enzymatic degradation, enabling prolonged circulation by increasing their half-life and sustainable targeted drug release, thus improving the pharmacokinetics efficacy.[132,170] The utilization of the delivery system increases the stability, solubility and biocompatibility of challenging therapeutics. Targeted drug delivery using nanomaterials minimizes the selection of resistant strains, and allows target organ accumulation by functionalized surface modification, thereby limiting systemic side effects and immunosuppression. Nanoparticles can also respond in the presence of certain exogenous stimuli, such as pH, enzymes and chemicals, leading to effective delivery of therapeutics in the bacterial microenvironment.[171,172]

5.2. Biofilm disruption

Biofilm disruption is the main therapeutic challenge because the EPS provides a barrier against antimicrobial agents. The deeper layers of the biofilm have low concentrations of oxygen and nutrients, promoting the growth of persister cells, thereby resulting in increased antimicrobial tolerance and resistance. Nanomaterials have a unique size that enables them to penetrate the EPS matrix of the biofilm. The smaller size and higher aspect ratio have greater penetration properties, which is most effective in the eradication of biofilms.[173,174] The surface charge properties of nanoparticles help in the efficient eradication of biofilm. The surface chemistry should be properly identified so that it leads to effective penetration into the biofilm. Stealth properties and biocompatibility through surface modifications make the nanoparticles more effective towards sufficient accumulation of nanomaterials inside the biofilm. Modifying the surface makes the nanoparticles more specific towards the biofilm. Anionic and zwitterionic nanoparticles have low EPS matrix penetration ability, whereas cationic nanoparticles with proper hydrophobicity can penetrate the EPS efficiently. Cationic nanoparticles can efficiently bind to the negatively charged matrix components due to the strong electrostatic force of attraction between the nanoparticles and the matrix.[175] The shape of the nanoparticles plays an important role in biofilm disruption. Spherical nanoparticles can penetrate the biofilm very easily, so it can be used to deliver therapeutics inside the biofilm.[176] Due to its small size, the diffusion of the nanocarrier carrying the therapeutic agent favors the killing of persister cells inside the biofilm matrix.[177] The shape also plays an important role in generating heat upon NIR irradiation due to localized plasmon resonance. When the temperature of such nanoparticles is raised inside the biofilm, it is sufficient to kill the bacteria inside the biofilm.[178] Nanomaterial penetration profiles are directly

related to the success of biofilm elimination. After entering the EPS matrix of the biofilm, nanomaterials kill the sessile and persister cells by their own antibacterial effect or by release of therapeutic agents in a similar fashion, as described earlier in biofilm inhibition. Polymeric and lipid nanoparticles loaded with antimicrobial agents effectively pass and disrupt the biofilms, resulting in the killing of the pathogens, whereas traditional antibiotics fail to perform.[146] Due to the distressing intramolecular forces, the AgNPs perturb the biofilm matrix.[179] Although AuNPs have very little or no antibacterial activity, functionalized AuNPs enhance the activity of antimicrobial agents by delivering the agents into the biofilm.[169] Micelles with surface charge can efficiently accumulate into the biofilm, showing significant destruction of the biofilm and bacteria within it.[139] In addition, nanomaterials deliver matrix-degrading enzymes, nuclease, and other small molecules inside the biofilm and disperse the EPS matrix.[180] Nanomaterials also inhibit the biofilm growth through interrupting the bacterial communication system, more specifically, the QS signaling pathway. Khan *et al.*[97] showed that ZnO nanospikes had the ability to inhibit the QS of *P. aeruginosa* and prevent biofilm formation. These nanospikes inhibit the QS signaling and also affect the production of virulence factors, which is necessary to form the biofilm. Altogether, the nanomaterials provide a unique way to combat the deadly bacterial infection, showing that several mechanisms of action, low therapeutic doses, and targeted delivery of drugs minimize bacterial resistance against nanoparticles.

6. Biomedical application of nanomaterials

Biofilm formation has been a major concern in the biomedical field since it may develop on surgical equipment, hospital beds, different medical implants, drug delivery devices, and most commonly on catheters. Besides the formation of the biofilm on the external substrates, the growth of biofilms also occurs on peripheral surfaces such as the wound bed. Biofilms may also form in internal organs, such as cardiovascular, dental, digestive, reproductive, respiratory, integumentary organs and the urinary system. According to the global report on sepsis by WHO, 24.4% mortality was reported among patients infected with health care-associated sepsis, which was increased to 52.3% among patients treated in ICUs.[181] To treat the biofilm-linked morbidity and mortality, replacement of the contaminated apparatus and treatment with antibiofilm agent remain mandatory. Surface coating on medical devices, including metal nanoparticles,[182,183] CNT,[184] GO and rGO,[185–188] has been one of the growing strategies to prevent biofilm colonization. Tran *et al.*[183] synthesized a formulation of silver nanoparticles conjugated with polydopamine (DA) and a biofilm-lysing enzyme (α-Amylase) to prevent the biofilm colonization on titanium substrates (Fig. 8A). The antibacterial effect of AgNPs denatured the bacterial cell wall and disintegrated the extracellular matrix of the *S. aureus* biofilm, thus reducing the biofilm biomass on the titanium substrate. Periprosthetic joint

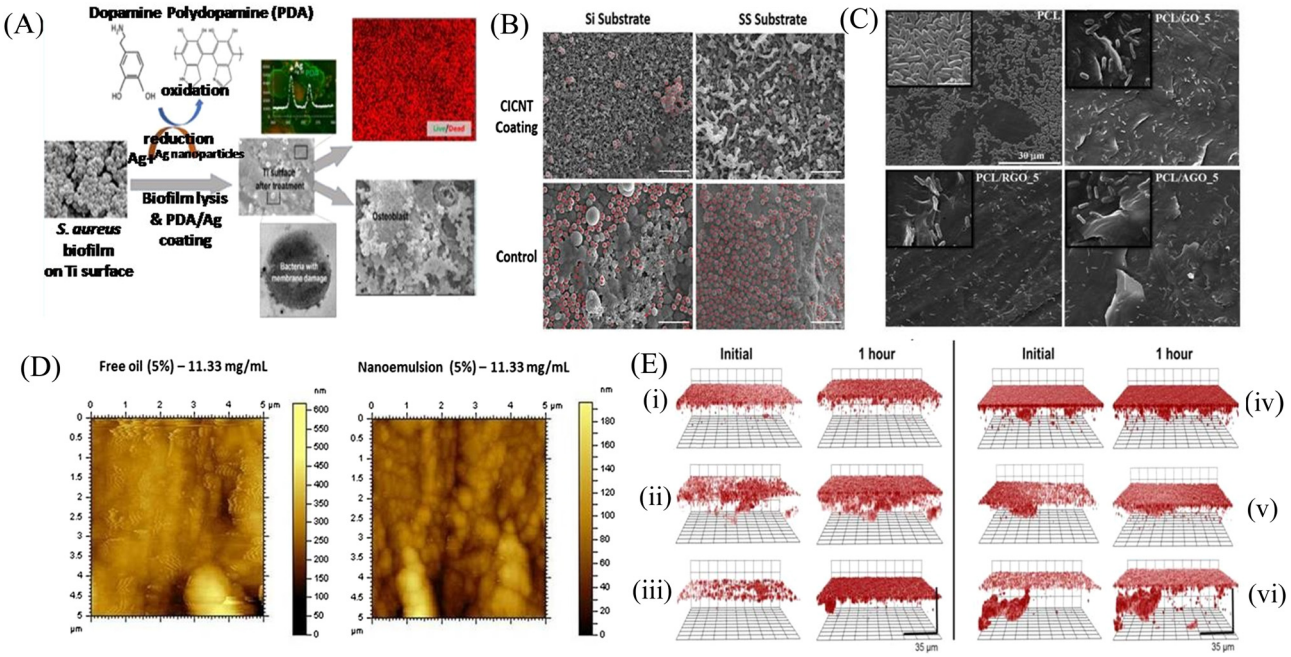

Fig. 8 (A) Schematic representation of the silver-based nanosystem. (B) MRSA cells marked in red for each material: CICNT-Si, CICNT-SS, carbon control, and SS control. Scale bars are 5 µm. CICNT-Si, carbon-infiltrated carbon nanotube-silicon; CICNT-SS, carbon-infiltrated carbon nanotube-stainless steel, MRSA. (C) SEM micrographs of biofilm formation on neat PCL, PCL/GO-5, PCL/RGO-5, and PCL/AGO-5 composite surfaces. (D) Influence of free oil and nanoemulsion treatments against the formation of biofilms of *P. aeruginosa*. (E) Confocal microscopy images of *S. aureus* biofilms exposed to 50 µg mL^{-1} RITC-tagged (i) G1 butyl, (ii) G2 butyl, (iii) G4 butyl, (iv) G1 hexyl, (v) G2 hexyl, and (vi) G4 hexyl dendrimers for 1 h. Initial images obtained approximately 5 min after dendrimer exposure. Threshold inverted for clarity. (A) Reprinted with permission from ref. 183. (B) Reprinted with permission from ref. 115. (C) Adapted with permission from ref. 186. (D) Reprinted with permission from ref. 189. (E) Reprinted with permission from ref. 190.

infections (PJI) associated with MRSA are caused due to orthopedic implant surgeries. MRSA biofilms in PJI are difficult to remove due to the poor penetration property of antibiotics. To overcome this limitation, CNT-coated medical devices were fabricated by Morco *et al.*[115] Following treatment of the MRSA biofilm with CICNT coatings for 48 h, there were 60–80% reductions of MRSA biofilm growth observed. Furthermore, FESEM images of the biofilm depicted that the CICNT treatment significantly reduced the biofilm biomass as compared to the untreated biofilm, and thus CICNT restricted the bacterial proliferation and bacterial growth (Fig. 8B). In another study, Kumar *et al.*[186] fabricated PCL composites consisting of graphene for orthopedic applications. PCL composites were fabricated with GO, rGO and amine-functionalized GO (AGO) with varied filler contents (1%–5%). Among all composites, AGO composites inhibited the biofilm growth. It was suggested that AGO with the synergistic role of oxygen and amine containing functional groups demonstrated improved modulus, stem cell proliferation, and biofilm inhibition suitable for orthopedic applications. The SEM image (Fig. 8C) demonstrated that PCL/GO_5, PCL/rGO_5, and PCL/AGO_5 nanocomposites prevented the biofilm formation. A thick bacterial biofilm was seen on the PCL surface. However, very little adhered bacteria were visible on the composite surfaces. Furthermore, Gundel *et al.*[189] synthesized a nanoemulsion consisting of Lemongrass oil having potential antimicrobial efficacy, antioxidant properties and antibiofouling efficacy. The essential oil nanoemulsion inhibited the biofilm formation of *P. aeruginosa* and *S. aureus* (Fig. 8D). Due to its efficacy as a strong antimicrobial agent, this nanoemulsion was found to be a better alternative to the conventional antibiofilm treatment. Worley *et al.*[190] developed dual-action NO-releasing alkyl chain-modified poly(amidoamine) dendrimers to study its antibiofilm efficacy against *S. aureus*, MRSA and *P. aeruginosa* biofilms. This alkyl chain-modified poly(amidoamine) dendrimer was fabricated with different generations (G1–G4), and was modified with butyl (short) or hexyl (medium) chains, along with their further modification with *N*-diazeniumdiolate NO donors. With the increase in the dendrimer size and functional group density, the antibiofilm efficacy of the NO-releasing dendrimers was enhanced. A combination of short and long alkyl chain modifications in the dendrimers had less toxicity at therapeutic levels with enhanced anti-biofilm activity along with NO release, implying synergistic advantage of conjugating multiple biocides on a single macromolecular scaffold. G1 hexyl and G4 hexyl dendrimers have shown excellent biofilm penetration in comparison to either G1 butyl or G4 butyl dendrimers in the *S. aureus* biofilm (Fig. 8E). Therefore, the hexyl-modified dendrimer exhibited better antibiofilm efficacies than the butyl-altered dendrimer due to their increased biofilm penetration, membrane intercalation and cell membrane damage. With the increase in the cellular membrane damage, there was more intracellular NO build up, leading to further increased antibiofilm activity without altering the cell membrane. Meeker *et al.*[191] synthesized gold nanocages (AuNC) and gold nanocages-coated polydopamine (AuNC@PDA). Furthermore, it was loaded with daptomycin (AuNC@Dap/PDA), and then finally conjugated with surface specific antibodies against staphylococcal protein A (aSpa) (AuNC@Dap/PDA-aSpa), which made it a highly photoactive and selective nanodrug against *S. aureus* (UAMS-1 and LAC strains). AuNC@PDA and AuNC@Dap/PDA exhibited a 3 log reduction of *S. aureus* upon irradiation of 808 nm laser due to the synergistic effect of both photothermal and antibiotics (Fig. 9A). Mai *et al.*[192] designed a cationic liposome-based delivery system augmented with photodynamic therapy for the effective treatment of burn infections. They developed a cationic lipid-mediated nanosinoporphyrin sodium (DVDMS) delivery system to examine the antimicrobial activity of cationic DVDMS-liposome (CDL)-conjugated with photodynamic antimicrobial chemotherapy (PACT) in both *P. aeruginosa* and its multidrug-resistant strain. The positively charged modified liposome accelerated the penetration of DVDMS inside *P. aeruginosa*. CDL-PACT caused ROS-mediated bacterial cell death, along with reduced virulence factor-related genes expression upon irradiation with a laser at 100 J cm^{-2}. Fluorescence imaging of CSDP hydrogen was seen both *in vitro* and *in vivo* (Fig. 9B). This nanosystem led to the complete removal of the bacterial infection by membrane permeabilization, damage, and then accelerated the wound healing cascade by decreasing the cytokines level in the presence of different growth factors, such as the bFGF, VEGF, TGF-β_1 and Hyp. Ashbaugh *et al.*[193] developed an excellent tunable antibiotic-loaded electrospun composite coating on the implant surface. This coating consists of poly(lactic-coglycolic acid) (PLGA) nanofibers embedded in a poly(ε-caprolactone) film to release combinatorial antibiotics (Van/Rif, Lin/Lin + Rif, and Dap/Dap + Rif) locally, and prevent chronic biofilm infection caused by MRSA. Van/Rif, Lin/Lin + Rif, and Dap/Dap + Rif combinations of antibiotic-loaded coatings were found to have strong antibiofouling efficacy to prevent biofilm formation in orthopedic implants (Fig. 9C). Patel *et al.*[194] fabricated a silver sulfadiazine-loaded solid lipid nanoparticles (SSD-SLNs) formulation, and supplemented it with chitosan gel and DNase-I for the effective treatment of *P. aeruginosa* biofilm-associated burn wounds. DNase-I accelerated the antibiotic susceptibility against *P. aeruginosa* biofilms by cleaving the eDNA, and thus eliminated the biofilm. Pure SSD and SSD-SLN were able to eradicate only 58.1% and 78.7% of biofilm after 72 h, respectively (Fig. 10A and B). After the addition of DNase I-incorporated SSD-SLN, there was an inhibition of around 96.8% of the *P. aeruginosa* biofilm. SSD-SLNs along with DNase-I from the *in vivo* wound healing study exhibited absolute wound healing after 21 days, but formulations of SSD and SSD-LSNs showed incomplete healing after 21 days. Wang *et al.*[195] fabricated a pH-switchable antimicrobial hydrogel by self-assembling of an octapeptide (Ac-Leu-Lys-Phe-Gln-Phe-His-Phe-Asp-NH_2, IKFQFHFD) with nanofiber networks encapsulated with cypate (photothermal agent) and proline (procollagen component) for the disruption of the biofilm of MRSA and acceleration of the wound healing process. This hydrogel was destabilized at an acidic pH value of 5.5, which led to the release of the peptide, cypate and proline. The released peptide

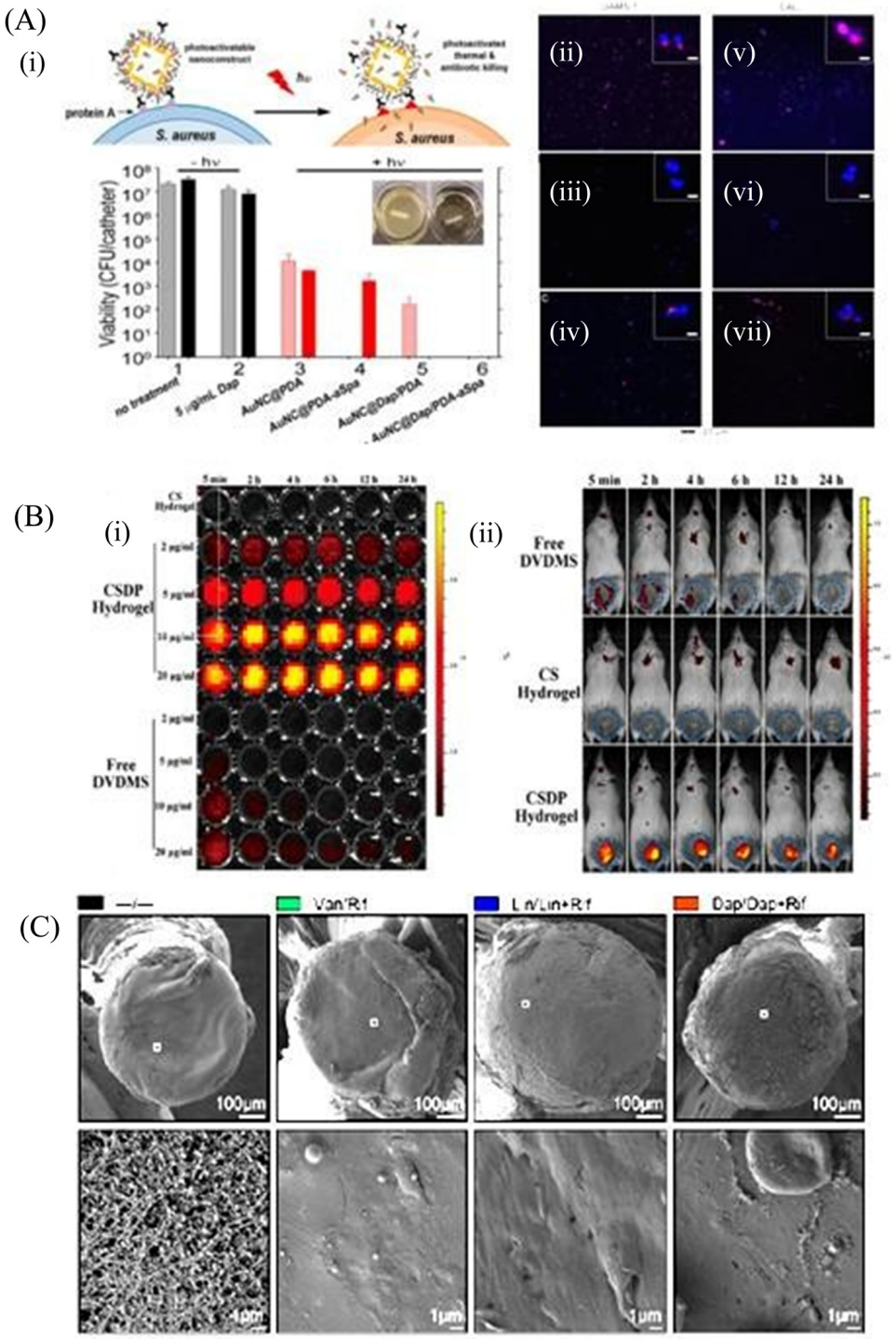

Fig. 9 (A) (i) Schematic illustration of the working mechanism of the targeted photoactivatable nanoconstruct for synergistic photothermal and antibiotic treatment of *S. aureus*. Two-photon fluorescence images of *S. aureus* cells treated at different conditions, (ii) UAMS-1 exposed to AuNC@PDA–aSpa, (iii) UAMS-1 exposed to AuNC@PDA, (iv) UAMS-1 *spa* mutant exposed to AuNC@PDA–aSpa, (v) LAC exposed to AuNC@PDA–aSpa, (vi) LAC treated with AuNC@PDA, (vii) LAC *spa* mutant exposed to AuNC@PDA–aSpa. Cells were stained with DAPI colored in blue. Luminescence of AuNCs was colored in red. (B) Fluorescence imaging of CSDP hydrogel (C) *In vivo* efficacy on eradication of infection and biofilm formation. Biofilm formation was assessed by SEM on *ex vivo* implants. (A) Reprinted with permission from ref. 191. (B) Adapted with permission from ref. 192. (C) Reprinted with permission from ref. 193.

IKFQFHFD demonstrated antibacterial efficacy by the cell wall and membrane disintegration, and cypate under NIR light irradiation (808 nm, power density of 0.5 W cm^{-2}) caused biofilm disruption by the photothermal activity. Furthermore, proline led to the acceleration of cell proliferation at the wound bed. The synergistic activity of the IKFQFHFD peptide and

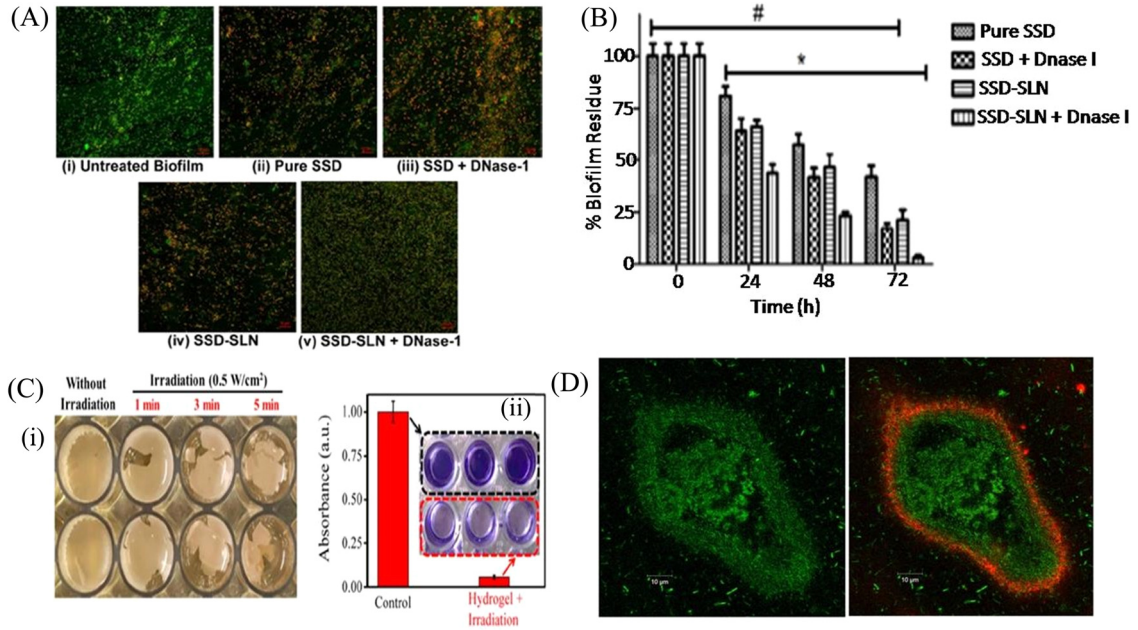

Fig. 10 (A) Laser scanning microscopy images of the *P. aeruginosa* biofilm treated with different test samples (40× magnification). Green fluorescent (SYTO 9) cells indicate the live bacterial cells, and red fluorescent (PI) cells indicate dead cells. (i) Untreated *P. aeruginosa* biofilm, (ii) Pure SSD, (iii) SSD + DNase-I, (iv) SSD-SLNs, and (v) SSD-SLNs + DNase-I (SSD equivalent to 18.75 μg mL^{-1} and DNase-I equivalent to 20 μg mL^{-1}). (B) Graph indicates the comparative inhibition of the established *P. aeruginosa* biofilm after three consecutive doses (once a day) of pure SSD or encapsulated SSD (18.75 μg mL^{-1}) with or without DNase-I (20 μg mL^{-1}). A repeated-measure two-way ANOVA was performed (*, $P < 0.05$, *versus* nontreated biofilms (0 h); #, $P < 0.05$, *versus* SSD-SLNs + DNase-I on 72 h). The viable count $2.3 \times 10^9 \pm 9.1 \times 10^7$ CFU mL^{-1} in the untreated biofilm was taken as one hundred percent. (C) (i) Representative photographs of integrated MRSA biofilm incubated with cypate released from the hydrogel-Cy system at scheduled time points of 4 h under a NIR laser (808 nm, 0.5 W cm^{-2}) irradiation for different times, (ii) crystal violet staining image and its corresponding absorbance for the integrated MRSA biofilm incubated with the hydrogel-Cy system (under pH 5.5) for 4 h followed by NIR laser irradiation (808 nm, 0.5 W cm^{-2}, 5 min). The biofilm under NIR laser irradiation without incubation with the hydrogel-Cy system was used as the control. (D) PAO1-GFP-tagged biofilm (green) grown in a flow cell (left) treated with octadecyl rhodamine B Chloride-tagged LCNPs (red). (A and B) Reprinted with permission from ref. 194. (C) Adapted with permission from ref. 195. (D) Reprinted with permission from ref. 197.

cypate of the hydrogel thus demonstrated efficient antibacterial and antibiofilm activity in infected wound care management. The *in vivo* studies suggested that this composite could heal diabetic mice within 20 days by complete removal of the MRSA biofilm. The results showed that the MRSA biofilm incubated with hydrogel-cypate system under NIR laser irradiation was completely eradicated, while irradiation alone or cypate with irradiation were not able to eradicate the biofilm completely (Fig. 10C). Fumakiya *et al.*[196] synthesized a topical nanomedicine for the controlled sustained release of LL37 (endogenous host defense peptide) and Serpin A1 (A1), an elastase inhibitor for chronic wound healing treatment. The combination of LL37 and A1 significantly promoted wound healing in BJ fibroblast cells and keratinocytes, eradicated bacterial contamination and inhibited biofilm formation by *S. aureus* and *E. coli*, and enhanced anti-inflammatory activity. For the first time, Thorn *et al.*[197] developed lipid liquid crystal nanoparticles (LCNPs) to enhance the antimicrobial and penetration property of tobramycin against *P. aeruginosa* in full-thickness wounds in mice. Tobramycin-LCNPs significantly reduced the bacterial colonization in the wound by 1000-fold more than individual tobramycin, which showed similar results as the untreated bacterial cells. SEM images (Fig. 10D) showed that red-labeled LCNP is coated over the GFP PAO1 biofilm.

7. Conclusion and future perspective

Biofilm formation by ESKAPE pathogens in the biomedical field has become difficult to treat due to the lack of effective conventional approaches. This is due to low penetration, enzymatic inactivation and degradation of antimicrobials in the microenvironment of biofilm. Nanomaterials have emerged as a novel strategy for the precise and effective treatment of bacterial biofilms. Because of their small size, nanomaterials can easily diffuse the EPS matrix of the biofilm and kill the persister and sessile cells through their intrinsic antibacterial activity and/or by delivering therapeutics. Nanomaterials interact with the bacterial cells and exhibit antibacterial activity through multiple pathways, which include ROS generation, damage of membrane and intracellular components, inhibition of protein synthesis and DNA replication. In addition, nanoparticles inhibit and disrupt biofilm formation through EPS and eDNA degradation, and interfere with the QS pathway. Even though nanotechnology has several advantages, it still has some limitations such as the cytotoxicity, effects on metabolism, poor renal clearance and aggregation with proteins and blood cells, causing health hazards. Dissolution of metal ions from nanoparticles waste also causes adverse health effects. Furthermore, the crossing of biological barriers and avoiding

the immune system to achieve targeted delivery are huge challenges. Many nanomaterials have been developed to combat the biofilm of ESKAPE pathogens, but the majority of them are confined to cell line and animal models. Clinical trials in humans are still limited. The undetermined side effects and expensive clinical trials need to be identified and taken care of. Development of appropriate antimicrobial nanomaterials need proper *in vitro* and *in vivo* models in respect to antibacterial, antibiofouling, biocompatibility and nanotoxicology. More specifically, an extensive study regarding the fundamental, pharmacological and biological properties of nanoparticles and its interaction with pathogens is needed for clinical development of nanomaterials. Few studies have been conducted *in vitro*, out of which few proceeded for animal trials with some of them chosen for human testing. Two nanoformulated liposomes are already in phase III trials, namely, Amikacin (Arikace™), for the treatment of chronic infection due to *P. aeruginosa* infection in cystic fibrosis patients,[198] and a nanoliposome-based formulation like Pulmaquin was prepared for the fast and sustained release of CIP.[199] All of these shortcomings of nanomaterials could be addressed by future investigation. In the coming years, the *in vivo* toxicity assays, animal studies and clinical trials may pave the way for combating the nanomaterial synthesis, stability and discard related issues. Thus, we conclude that the nanomaterials may provide an excellent opportunity to combat biofilm-related infections caused by ESKAPE pathogens by minimizing the selection of resistance through the delivery of therapeutics with sub-inhibitory doses and killing of bacteria by multiple bactericidal pathways. The development of nanomaterials as antimicrobials and delivery agents requires the collaboration from scientists of different fields, such as biomedical researchers, microbiologists, chemists and engineers. This will lead to the successful generation and commercialization of nanomaterials, which will bring a revolutionary impact to treat biofilm-related infections.

Author contributions

Arpita Mukherjee: investigation, formal analysis, writing – original draft, writing – review & editing. Somashree Bose: resources, data curation, visualization, and writing – original draft. Anirban Shaoo: resources, visualization, Sujoy K. Das: conceptualization, supervision, validation, funding acquisition, project administration, writing – review & editing.

Conflicts of interest

The authors declare no conflicts of interest.

Acknowledgements

The financial support received from Science and Engineering Research Board (SERB), Govt. of India under Core Research Grant (CRG/2018/002307) is gratefully acknowledged. A. M. and S. B. gratefully acknowledge UGC, Govt. of India for fellowships.

References

1 https://emerypharma.com/blog/eskape-pathogens-explained.
2 D. Sharma, L. Misba and A. U. Khan, *Antimicrob. Res. Infect. Control*, 2019, **8**, 76.
3 Z. Jia, *Antifouling Strategies-Interference with Bacterial Adhesion*, *IntechOpen*, United Kingdom, 2022, vol. 14, p. 392.
4 D. M. P. De Oliveira, B. M. Forde, T. J. Kidd, N. A. H. Patrick, M. A. Schembri, S. A. Beatson, D. L. Paterson and M. J. Walker, *Clin. Microbiol. Rev.*, 2020, **33**, 181.
5 O. Ciofu and T. Tolker-Nielsen, *Front. Microbiol.*, 2019, **10**, 913.
6 R. M. Donlan, *Emerging Infect. Dis.*, 2002, **8**, 881.
7 V. G. Preda and O. Săndulescu, *Discoveries*, 2019, **7**, 100.
8 N. Baig, I. Kammakakam and W. Falath, *Mater. Adv.*, 2021, **2**, 1821.
9 Y. N. Slavin, J. Asnis, U. O. Häfeli and H. Bach, *J. Nanobiotechnol.*, 2017, **15**, 65.
10 Q. L. Feng, J. Wu, G. Q. Chen, F. Z. Cui, T. N. Kim and J. O. Kim, *J. Biomed. Mater. Res.*, 2000, **52**, 662.
11 J. K. Patra, G. Das, L. F. Fraceto, E. V. R. Campos, M. D. P. Rodriguez-Torres, L. S. Acosta-Torres, L. A. Diaz-Torres, R. Grillo, M. K. Swamy, S. Sharma, S. Habtemariam and H. S. Shin, *J. Nanobiotechnol.*, 2018, **16**, 71.
12 H. C. Flemming and J. Wingender, *Nat. Rev. Microbiol.*, 2010, **8**, 623.
13 S. Veerachamy, T. Yarlagadda, G. Manivasagam and P. K. Yarlagadda, *Proc. Inst. Mech. Eng., Part H*, 2014, **228**, 1083.
14 G. Reid, *Int. J. Antimicrob. Agents*, 1999, **11**, 223.
15 N. K. Archer, M. J. Mazaitis, J. W. Costerton, J. G. Leid, M. E. Powers and M. E. Shirtliff, *Virulence*, 2011, **2**, 445.
16 L. D. Blackman, Y. Qu, P. Cass and K. E. S. Locock, *Chem. Soc. Rev.*, 2021, **50**, 1587.
17 C. G. Kumar and S. K. Anand, *Int. J. Food Microbiol.*, 1998, **42**, 9.
18 S. Park, M. Lee, J. Kim, H. Kim, M. Jung, M. Shin, W. Lee, G. Cheong, J. R. Lee and M. Jang, *Molecules*, 2019, **24**, 4560.
19 M. Thoendel and A. R. Horswill, *Adv. Appl. Microbiol.*, 2010, **71**, 91.
20 K. Papenfort and B. L. Bassler, *Nat. Rev. Microbiol.*, 2016, **14**, 576.
21 F. L. Paganelli, R. J. Willems, P. Jansen, A. Hendrickx, X. Zhang, M. J. M. Bonten and H. L. Leavis, *mBio*, 2013, **4**, e00154.
22 J. Top, F. L. Paganelli, X. Zhang, W. V. Schaik, H. L. Leavis, M. V. Luit-Asbroek, T. V. D. Poll, M. Leendertse, M. J. M. Bonten and R. J. L. Willems, *PLoS One*, 2013, **8**, 65224.
23 D. I. Johnson, *Bacterial Pathogens and Their Virulence Factors. Enterococcus spp.*, *Springer*, Cham, 2018, ch. 5, p. 81.
24 C. R. Arciola, D. Campoccia, S. Ravaioli and L. Montanaro, *Front. Cell. Infect. Microbiol.*, 2015, **5**, 7.
25 A. M. S. Figueiredo, F. A. Ferreira, C. O. Beltrame and M. F. Côrtes, *Crit. Rev. Microbiol.*, 2017, **43**, 602.

26 J. L. Lister and A. R. Horswill, *Front. Cell. Infect. Microbiol.*, 2014, **4**, 178.
27 J. M. Yarwood, D. J. Bartels, E. M. Volper and E. P. Greenberg, *J. Bacteriol.*, 2004, **186**, 1838.
28 J. Pratten, S. J. Foster, P. F. Chan, M. Wilson and S. P. Nair, *Microbes Infect.*, 2001, **3**, 633.
29 M. Habash and G. Reid, *J. Clin. Pharmacol.*, 1999, **39**, 887.
30 J. X. Zheng, Z. W. Lin, C. Chen, Z. Chen, F. J. Lin, Y. Wu, S. Y. Yang, X. Sun, W. M. Yao, D. Y. Li, Z. J. Yu, J. L. Jin, D. Qu and Q. W. Deng, *Front. Cell. Infect. Microbiol.*, 2018, **8**, 21.
31 T. Pacheco, A. É. I. Gomes, N. M. G. Siqueira, L. Assoni, M. Darrieux, H. Venter and L. F. C. Ferraz, *Front. Microbiol.*, 2021, **12**, 597735.
32 H. Nirwati, K. Sinanjung, F. Fahrunissa, F. Wijaya, S. Napitupulu, V. P. Hati, M. S. Hakim, A. Meliala, A. T. Aman and T. Nuryastuti, *BMC Proc.*, 2019, **13**, 20.
33 H. Zeighami, F. Valadkhani, R. Shapouri, E. Samadi and F. Haghi, *BMC Infect. Dis.*, 2019, **19**, 629.
34 C. Cucarella, C. Solano, J. Valle, B. Amorena, I. Lasa and J. R. Penadés, *J. Bacteriol.*, 2001, **183**, 2888.
35 A. M. Asaad, S. Ansari, S. E. Ajlan and S. M. Awad, *Infect. Drug Resist.*, 2021, **14**, 709.
36 X. Sun, Z. Ni, J. Tang, Y. Ding, X. Wang and F. Li, *Front. Microbiol.*, 2021, **12**, 679241.
37 M. López-Martín, J. F. Dubern, M. R. Alexander and P. Williams, *J. Bacteriol.*, 2021, **203**, 635.
38 M. T. T. Thi, D. Wibowo and B. H. A. Rehm, *Int. J. Mol. Sci.*, 2020, **21**, 8671.
39 N. B. Cabra, B. Paetzold, T. Ferrar, R. Mazzolini, E. Torrents, L. Serrano and M. L. Luch-Sena, *Sci. Rep.*, 2020, **10**, 9390.
40 P. Owlia, R. Nosrati, R. Alaghehbandan and A. R. Lari, *GMS Hyg. Infect. Control*, 2014, **9**, Doc13, DOI: **10.3205/dgkh000233**.
41 R. S. Smith, S. G. Harris, R. Phipps and B. Iglewski, *J. Bacteriol.*, 2002, **184**, 1132.
42 J. Tang, Y. Chen, X. Wang, Y. Ding, X. Sun and Z. Ni, *Infect. Drug Resist.*, 2020, **13**, 4273.
43 K. Oinuma and E. P. Greenberg, *J. Bacteriol.*, 2011, **193**, 421.
44 J. S. Bustos, M. A. Ares, C. A. G. Aldapa, J. A. G. Y. Merchand, J. A. Girón and M. A. D. L. Cruz, *Front. Microbiol.*, 2020, **11**, 560488.
45 V. C. Kalia, *Biotechnol. Adv.*, 2013, **31**, 224.
46 H. Koo, R. N. Allan, R. P. Howlin, P. Stoodley and L. Hall-Stoodley, *Nat. Rev. Microbiol.*, 2017, **15**, 740.
47 X. Luo, B. Zhang, Y. Lu, Y. Mei and L. Shen, *J. Hazard. Mater.*, 2022, **421**, 126682.
48 S. L. Munasur, E. B. Turawa, C. U. M. E. Chikte and A. Musekiwa, *Int. J. Environ. Res. Public Health*, 2020, **17**, 5601.
49 C. B. Lineback, C. A. Nkemngong, S. T. Wu, X. Li, P. J. Teska and H. F. Oliver, *Antimicrob. Res. Infect. Control*, 2018, **7**, 154.
50 G. Orrù, S. D. Nero, E. Tuveri, M. L. Ciusa, F. Pilia, M. Erriu, G. Orrù, M. Liciardi, V. Piras and G. Denotti, *Open Dent. J.*, 2010, **4**, 140.
51 F. Natalio, R. André, A. F. Hartog, B. Stoll, K. P. Jochum, R. Wever and W. Tremel, *Nat. Nanotechnol.*, 2012, **7**, 530.
52 S. Nadar, T. Khan, S. G. Patching and A. Omri, *Microorganisms*, 2022, **10**, 303.
53 N. Ooi, K. Miller, C. Randall, W. Rhys-Williams, W. Love and I. Chopra, *J. Antimicrob. Chemother.*, 2010, **65**, 72.
54 K. Murakami, H. Yumoto, A. Murakami, T. Amoh, D. Viducic, K. Hirota, A. Tabat, H. Nagamune, H. Kourai, T. Matsuo and Y. Miyake, *J. Appl. Microbiol.*, 2017, **122**, 893.
55 C. Wu, J. Y. Lim, G. G. Fuller and L. Cegelski, *Langmuir*, 2013, **29**, 920.
56 C. M. Toutain-Kidd, S. C. Kadivar, C. T. Bramante, S. A. Bobin and M. E. Zegans, *Antimicrob. Agents Chemother.*, 2009, **53**, 136.
57 B. V. G. Nguyen, T. Nagakubo, M. Toyofuku, N. Nomura and A. S. Utada, *Langmuir*, 2020, **36**, 6411.
58 R. Watanabe, T. Matsumoto, G. Sano, Y. Ishii, K. Tateda, Y. Sumiyama, J. Uchiyama, S. Sakurai, S. Matsuzaki, S. Imai and K. Yamaguchi, *Antimicrob. Agents Chemother.*, 2007, **51**, 446.
59 L. G. Kifelew, M. S. Warner, S. Morales, L. Vaughan, R. Woodman, R. Fitridge, J. G. Mitchell and P. Speck, *BMC Microbiol.*, 2020, **20**, 204.
60 B. Sisakhtpour, A. Mirzaei, V. Karbasizadeh, N. Hosseini, M. Shabani and S. Moghim, *Ann. Clin. Microbiol. Antimicrob.*, 2022, **21**, 1.
61 M. M. Quinn, P. K. Henneberger, B. Braun, G. L. Delclos, K. Fagan, V. Huang, J. L. Knaack, L. Kusek, S. J. Lee, N. Le Moual, K. A. Maher, S. H. Mc Crone, A. H. Mitchell, E. Pechter, K. Rosenman, L. Sehulster, A. C. Stephens, S. Wilburn and J. P. Zock, *Am. J. Infect. Control*, 2015, **43**, 424.
62 A. Bridier, R. Briandet, V. Thomas and F. Dubois-Brissonnet, *Biofouling*, 2011, **27**, 1017.
63 E. Rojo-Molinero, M. D. Macia, R. Rubio, B. Moya, G. Cabot, C. Lopez-Causap, J. L. Pérez, R. Cantón and A. Oliver, *Antimicrob. Agents Chemother.*, 2016, **60**, 2912.
64 C. Watanakunakorn, *Rev. Infect. Dis.*, 1981, **3**, 210.
65 T. Heinonen, S. Hargraves, M. Georgieva, C. Widmann, N. Jacquier and J. Glob, *Antimicrob. Resist.*, 2021, **25**, 227.
66 R. Festa, R. L. Ambrosio, A. Lamas, L. Gratino, G. Palmieri, C. M. Franco, A. Cepedaa and A. Anastasio, *Foods*, 2021, **10**, 1372.
67 **https://www.cdc.gov/drugresistance/about/how-resistance-happens.html**.
68 T. Parandhaman, M. D. Dey and S. K. Das, *Green Chem.*, 2019, **21**, 5469.
69 S. A. A. Rizvi and A. M. Saleh, *Saudi Pharm. J.*, 2018, **26**, 64.
70 L. Wang, C. Hu and L. Shao, *Int. J. Nanomed.*, 2017, **12**, 1227.
71 H. Lan and D. Ph, The Use of Nanoparticles to Prevent and Eliminate Bacterial Biofilms, 2017, **344**.
72 S. N. Kłodzińska, F. Wan, H. Jumaa, C. Sternberg, T. Rades and H. M. Nielsen, *J. Colloid Interface Sci.*, 2019, **555**, 595.
73 G. Sanità, B. Carrese and A. Lamberti, *Front. Mol. Biosci.*, 2020, **7**, 381.

74 A. Bahrami, R. Delshadi and S. M. Jafari, *Trends Food Sci. Technol.*, 2020, **99**, 217.
75 S. A. Masurkar, P. R. Chaudhari, V. B. Shidore and S. P. Kamble, *IET Nanobiotechnol.*, 2012, **6**, 110.
76 Prateeksha, B. R. Singh, M. Shoeb, S. Sharma, A. H. Naqvi, V. K. Gupta and B. N. Singh, *Front. Cell. Infect. Microbiol.*, 2017, **7**, 93.
77 N. A. Al-Shabib, F. M. Husain, F. Ahmed, R. A. Khan, I. Ahmad, E. Alsharaeh, M. S. Khan, A. Hussain, Md. T. Rehman, M. Yusuf, I. Hassan, J. M. Khan, G. Md Ashraf, A. Alsalme, M. F. Al-Ajmi, V. V. Tarasov and G. Aliev, *Sci. Rep.*, 2016, **6**, 36761.
78 Y. Chen, Z. Fan, Z. Zhang, W. Niu, C. Li, N. Yang, B. Chen and H. Zhang, *Chem. Rev.*, 2018, **118**, 6409.
79 L. Wang, C. Hu and L. Shao, *Int. J. Nanomed.*, 2017, **12**, 1227.
80 E. S. López, D. Gomes, G. Esteruelas, L. Bonilla, A. L. L. Machado, R. Galindo, A. Cano, M. Espina, M. Ettcheto, A. Camins, A. M. Silva, A. Durazzo, A. Santini, M. L. Garcia and E. B. Souto, *Nanomaterials*, 2020, **10**, 292.
81 T. Ameh, M. Gibb, D. Stevens, S. H. Pradhan, E. Braswell and C. M. Sayes, *Nanomaterials*, 2022, **12**, 2402.
82 J. M. V. Makabenta, A. Nabawy, C. H. Li, S. Schmidt-Malan, R. Patel and V. M. Rotello, *Nat. Rev. Microbiol.*, 2021, **19**, 23.
83 M. H. Siddique, B. Aslam, M. Imran, A. Ashraf, H. Nadeem, S. Hayat, M. Khurshid, M. Afzal, I. R. Malik, M. Shahzad, U. Qureshi, Z. U. H. Khan and S. Muzammi, *BioMed Res. Int.*, 2020, 6398165.
84 Z. Qiao, Y. Yao, S. Song, M. Yin, M. Yang, D. Yan, L. Yang and J. Luo, *J. Mater. Chem. B*, 2020, **8**, 3138.
85 F. Khan, P. Manivasagan, J. W. Lee, D. T. N. Pham, J. Oh and Y. M. Kim, *Mar. Drugs*, 2019, **17**, 208.
86 B. Wan, Y. Zhu, J. Tao, F. Zhu, J. Chen, L. Li, J. Zhao, L. Wang, S. Sun, Y. Yang, X. Zhang and Y. Zhang, *ACS Appl. Mater. Interfaces*, 2020, **12**, 9050.
87 X. Wang, J. Wu, P. Li, L. Wang, J. Zhou, G. Zhang, X. Li, B. Hu and X. Xing, *ACS Appl. Mater. Interfaces*, 2018, **10**, 34905.
88 S. Kannan, A. Solomon, G. Krishnamoorthy and M. Marudhamuthu, *Sci. Rep.*, 2021, **11**, 1102.
89 M. S. Usman, M. E. E. Zowalaty, K. Shameli, N. Zainuddin, M. Salama and N. A. Ibrahim, *Int. J. Nanomed.*, 2013, **8**, 4467.
90 T. Amna, M. S. Hassan, N. A. Barakat, D. R. Pandeya, S. T. Hong, M. S. Khil and H. Y. Kim, *Appl. Microbiol. Biotechnol.*, 2012, **93**, 743.
91 S. V. Gudkov, D. E. Burmistrov, V. V. Smirnova, A. A. Semenova and A. B. Lisitsyn, *Nanomaterials*, 2022, **12**, 2635.
92 J. H. Kim, H. Cho, S. E. Ryu and M. U. Choi, *Arch. Biochem. Biophys.*, 2000, **382**, 72.
93 M. Altaf, M. T. Zeyad, M. A. Hashmi, S. Manoharadas, S. A. Hussain, M. S. Ali Abuhasil and M. A. M. Almuzaini, *RSC Adv.*, 2021, **11**, 19248.
94 N. Tran, A. Mir, D. Mallik, A. Sinha, S. Nayar and T. J. Webster, *Int. J. Nanomed.*, 2010, **5**, 277.
95 S. R. Dwivedi, F. Wahab Khan, Y. K. Mishra, J. Musarrat and A. A. Al-Khedhairy, *PLoS One*, 2014, **9**, 111289.
96 N. N. M. Adnan, Z. Sadrearhami, A. Bagheri, T. K. Nguyen, E. H. H. Wong, K. K. K. Ho, M. Lim, N. Kumar and C. Boyer, *Macromol. Rapid Commun.*, 2018, **39**, 1800159.
97 M. F. Khan, F. M. Husain, Q. Zia, E. Ahmad, A. Jamal, M. Alaidarous, S. Banawas, M. M. Alam, B. A. Alshehri, M. Jameel, P. Alam, M. I. Ahamed, A. H. Ansari and I. Ahmad, *ACS Omega*, 2020, **5**, 32203.
98 B. Tian, S. Tang, C. Wang, W. Wang, C. Wu, Y. Guo, Y. Guo and Z. Zhu, *Colloids Surf., B*, 2014, **123**, 403.
99 S. Begum, A. Pramanik, D. Davis, S. Patibandla, K. Gates, Y. Gao and P. C. Ray, *ACS Omega*, 2020, **5**, 3116.
100 Z. L. Shaw, S. Kuriakose, S. Cheeseman, M. D. Dickey, J. Genzer, A. J. Christofferson, R. J. Crawford, C. F. McConville, J. Chapman, V. K. Truong, A. Elbourne and S. Walia, *Nat. Commun.*, 2021, **12**, 3897.
101 S. Pandit, K. Gaska, V. R. S. S. Mokkapati, S. Forsberg, M. Svensson, R. Kádár and I. Mijakovic, *RSC Adv.*, 2019, **9**, 33454.
102 N. Qureshi, R. Patil, M. Shinde, G. Umarji, V. Causin, W. Gade, U. Mulik, A. Bhalerao and D. P. Amalnerkar, *Appl. Nanosci.*, 2015, **5**, 331.
103 R. Žalnėravičius, V. Klimas, A. Paškevičius, G. Grincienė, R. Karpicz, A. Jagminas and A. Ramanavičius, *J. Colloid Interface*, 2021, **591**, 115.
104 X. Zhang, W. Zhang, L. Liu, M. Yang, L. Huang, K. Chen, R. Wang, B. Yang, D. Zhang and J. Wang, *Nanotechnology*, 2017, **28**, 225101.
105 P. Choudhary, B. Ramalingam and S. K. Das, *ACS Biomater. Sci. Eng.*, 2020, **6**, 5911.
106 F. Lin, C. Li and Z. Chen, *Front. Microbiol.*, 2018, **9**, 259.
107 P. Li, S. Liu, G. Zhang, X. Yang, W. Cao, X. Gong and X. Xing, *ACS Appl. Bio Mater.*, 2020, **3**, 1105.
108 M. Ritenberg, S. Nandi, S. Kolusheva, R. Dandela, M. M. Meijler and R. Jelinek, *ACS Chem. Biol.*, 2016, **11**, 1265.
109 G. Liang, H. Shi, Y. Qi, J. Li, A. Jing, Q. Liu, W. Feng, G. Li and S. Gao, *Int. J. Nanomed.*, 2020, **15**, 5473.
110 H. Wang, Z. Song, J. Gu, S. Li, Y. Wu and H. Han, *ACS Biomater. Sci. Eng.*, 2019, **5**, 4739.
111 P. Li, S. Liu, W. Cao, G. Zhang, X. Yang, X. Gong and X. Xing, *Chem. Commun.*, 2020, **56**, 2316.
112 I. Malek, C. F. Schaber, T. Heinlein, J. J. Schneider, S. N. Gorb and R. A. Schmitz, *J. Mater. Chem. B*, 2016, **4**, 5228.
113 R. T. Santos, M. Gomes, L. C. Gomes and F. J. Mergulhao, *iScience*, 2020, **24**, 102001.
114 S. Kang, M. S. Mauter and M. Elimelech, *Environ. Sci. Technol.*, 2008, **42**, 7528.
115 S. R. Morco, D. L. Williams, B. D. Jensen and A. E. Bowden, *J. Orthop. Res.*, 2022, **40**, 1953.
116 H. Fallatah, M. Elhaneid, H. Ali-Boucetta, T. W. Overton, H. El Kadri and K. Gkatzionis, *Environ. Sci. Pollut. Res. Int.*, 2019, **26**, 25057.
117 X. Dai, Y. Zhao, Y. Yu, X. Chen, X. Wei, X. Zhang and C. Li, *Nanoscale*, 2018, **10**, 18520.
118 K. Yuan, B. Jurado-Sánchez and A. Escarpa, *Angew. Chem., Int. Ed.*, 2021, **60**, 4915.

119 T. Parandhaman, P. Choudhary, B. Ramalingam, M. Schmidt, S. Janardhanam and S. K. Das, *ACS Biomater. Sci. Eng.*, 2021, **7**, 5899.
120 P. Choudhary, B. Ramalingam and S. K. Das, *ACS Biomater. Sci. Eng.*, 2020, **6**, 5911.
121 R. Banerjee, *J. Biomater. Appl.*, 2001, **16**, 3.
122 Z. Drulis-Kawa and A. Dorotkiewicz-Jach, *Int. J. Pharm.*, 2010, **387**, 187.
123 Y. Hou, Z. Wang, P. Zhang, H. Bai, Y. Sun, J. Duan and H. Mu, *Int. J. Mol. Sci.*, 2017, **9**, 784.
124 D. Dong, N. Thomas, B. Thierry, S. Vreugde, C. A. Prestidge and P. J. Wormald, *PLoS One*, 2015, **10**, 131806.
125 Y. Zhao, X. Dai, X. Wei, Y. Yu, X. Chen, X. Zhang and C. Li, *ACS Appl. Mater. Interfaces*, 2018, **10**, 14426.
126 G. Mi, D. Shi, M. Wang and T. J. Webster, *Adv. Healthcare Mater.*, 2018, **7**, 1800103.
127 E. B. Souto, I. Baldim, W. P. Oliveira, R. Rao, N. Yadav, F. M. Gama and S. Mahant, *Expert Opin. Drug Delivery*, 2020, **17**, 357.
128 B. Rodenak-Kladniew, S. Scioli Montoto, M. L. Sbaraglini, M. Di Ianni, M. E. Ruiz, A. Talevi, V. A. Alvarez, N. Durán, G. R. Castro and G. A. Islan, *Int. J. Pharm.*, 2019, **569**, 118575.
129 A. Alalaiwe, P. W. Wang, P. Lu, Y. Chen, J. Fang and S. Yan, *Front. Microbiol.*, 2018, **9**, 1493.
130 Md. M. Anjum, K. K. Patel, D. Dehari, N. Pandey, R. Tilak, A. K. Agrawal and S. Singh, *Drug Delivery Transl. Res.*, 2021, **11**, 305.
131 L. Luan, Z. Chi and C. Liu, *Nanomaterials*, 2019, **9**, 763.
132 C. Sahli, S. E. Moya, J. S. Lomas, C. Gravier-Pelletier, R. Briandet and M. Hémadi, *Theranostics*, 2022, **12**, 2383.
133 S. Perumal, R. Atchudan and W. Lee, *Polymers*, 2022, **14**, 2510.
134 Y. Xi, T. Song, S. Tang, N. Wang and J. Du, *Biomacromolecules*, 2016, **17**, 3922.
135 B. Hisey, P. J. Ragogna and E. R. Gillies, *Biomacromolecules*, 2017, **18**, 914.
136 J. Qiao, M. Purro, Z. Liu and M. P. Xiong, *ACS Infect. Dis.*, 2018, **4**, 1346.
137 S. C. Park, C. Ko, H. Hyeon, M. K. Jang and D. Lee, *ACS Appl. Mater. Interfaces*, 2020, **12**, 54306.
138 R. Guo, K. Li, B. Tian, C. Wang, X. Chen, X. Jiang, H. He and W. Hong, *J. Nanobiotechnol.*, 2021, **19**, 232.
139 M. Chen, S. Xie, J. Wei, X. Song, Z. Ding and X. Li, *ACS Appl. Mater. Interfaces*, 2018, **10**, 36814.
140 F. Najafi, M. Salami-Kalajahi and H. Roghani-Mamaqani, *J. Iran. Chem. Soc.*, 2021, **18**, 503.
141 A. Felczak, N. Wrońska, A. Janaszewska, B. Klajnert, M. Bryszewska, D. Appelhans, B. Voit, S. Rozalskaa and K. Lisowska, *New J. Chem.*, 2012, **36**, 2215.
142 A. A. Bahar, Z. Liu, F. Totsingan, C. Buitrago, N. Kallenbach and D. Ren, *Appl. Microbiol. Biotechnol.*, 2015, **99**, 8125.
143 E. M. V. Johansson, S. A. Crusz, E. Kolomiets, L. Buts, R. U. Kadam, M. Cacciarini, K. Bartels, S. P. Diggle, M. Cámara, P. Williams, R. Loris, C. Nativi, F. Rosenau, K. Jaeger, T. Darbre and J. Reymond, *Chem. Biol.*, 2008, **15**, 1249.
144 J. Fernandez, Á. Martin-Serrano, N. Gómez-Casanova, A. Falanga, S. Galdiero, F. J. de la Mata, I. Heredero-Bermejo and P. Ortega, *Polymers*, 2021, **13**, 2127.
145 K. Winnicka, M. Wroblewska, P. Wieczorek, P. T. Sacha and E. A. Tryniszewska, *Molecules*, 2013, **18**, 8607.
146 D. E. Discher and F. Ahmed, *Annu. Rev. Biomed. Eng.*, 2006, **8**, 323.
147 Y. Xi, Y. Wang, J. Gao, Y. Xiao and J. Du, *ACS Nano*, 2019, **13**, 13645.
148 Y. Hong, Y. Xi, J. Zhang, D. Wang, H. Zhang, N. Yan, S. He and J. Du, *J. Mater. Chem. B*, 2018, **6**, 6311.
149 P. Walvekar, R. Gannimani, M. Salih, S. Makhathini, C. Mocktar and T. Govender, *Colloids Surf., B*, 2019, **182**, 110388.
150 H. Wang, X. Nie, W. You, W. Huang, G. Chen, F. Gao, L. Xia, L. Zhang, L. Wang, A. Shen, K. Wu, S. Ding and Y. You, *ACS Appl. Mater. Interfaces*, 2021, **13**, 56838.
151 A. Gupta, A. Z. Md Badruddoza and P. S. Doyle, *Langmuir*, 2017, **33**, 7118.
152 P. Prateeksha, S. K. Barik and B. N. Singh, *Sci. Rep.*, 2019, **9**, 6520.
153 K. Ramalingam and V. A. Lee, *Artif. Cells, Nanomed., Biotechnol.*, 2018, **46**, 737.
154 Y. Oz, A. Nabawy, S. Fedeli, A. Gupta, R. Huang, A. Sanyal and V. M. Rotello, *ACS Appl. Mater. Interfaces*, 2021, **13**, 40325.
155 C. Li, R. F. Landis, J. M. Makabenta, A. Nabawy, T. Tronchet, D. Archambault, Y. Liu, R. Huang, M. Golan, W. Cui, J. Mager, A. Gupta, S. Schmidt-Malan, R. Patel and V. M. Rotello, *Mater. Horiz.*, 2021, **8**, 1776.
156 Z. Song, H. Sun, Y. Yang, H. Jing, L. Yang, Y. Tong, C. Wei, Z. Wang, Q. Zou and H. Zeng, *Nanomedicine*, 2016, **12**, 1543.
157 Y. Y. Hwang, K. Ramalingam, D. R. Bienek, V. Lee, T. You and R. Alvarez, *Antimicrob. Agents Chemother.*, 2013, **57**, 3568.
158 S. K. Das, D. Kumar, S. Swarnakar, S. Bose and Y. Dahat, A Novel Composition of Cationic Metal Nanoparticle Conjugated Nanoemulsion and a Process for the Preparation Thereof, *India Pat.*, 202111045225, 2021.
159 F. Hizal, I. Zhuk, S. Sukhishvili, H. J. Busscher, H. C. van der Mei and C. H. Choi, *ACS Appl. Mater. Interfaces*, 2015, **7**, 20304.
160 O. Bondarenko, A. Ivask, A. Käkinen, I. Kurvet and A. Kahru, *PLoS One*, 2013, **8**, 64060.
161 J. S. Kim, E. Kuk, K. N. Yu, J. H. Kim, S. J. Park, H. J. Lee, S. H. Kim, Y. K. Park, Y. H. Park, C. Y. Hwang, Y. K. Kim, Y. S. Lee, D. H. Jeong and M. H. Cho, *Nanomedicine*, 2007, **3**, 95.
162 O. Gordon, T. V. Slenters, P. S. Brunetto, A. E. Villaruz, D. E. Sturdevant, M. Otto, R. Landmann and K. M. Fromm, *Antimicrob. Agents Chemother.*, 2010, **54**, 4208.
163 W. Hu, M. R. Younis, Y. Zhou, C. Wang and X. H. Xia, *Small*, 2020, **16**, 2000553.

164 Z. Chen, J. J. Yin, Y. T. Zhou, Y. Zhang, L. Song, M. Song, S. Hu and N. Gu, *ACS Nano*, 2012, **6**, 4001.
165 S. Singh, *Front. Chem.*, 2019, **7**, 46.
166 C. N. Lok, C. M. Ho, R. Chen, Q. He, W. Yu, H. Sun, P. K. Tam, J. Chiu and C. Che, *J. Biol. Inorg. Chem.*, 2007, **12**, 527.
167 S. Kang, M. Herzberg, D. F. Rodrigues and M. Elimelech, *Langmuir*, 2008, **24**, 6409.
168 G. E. Valenti, S. Alfei, D. Caviglia, C. Domenicotti and B. Marengo, *Int. J. Mol. Sci.*, 2022, **23**, 6108.
169 Y. Zhao, Y. Tian, Y. Cui, W. Liu, W. Ma and X. Jiang, *J. Am. Chem. Soc.*, 2010, **132**, 12349.
170 S. A. A. Rizvi and A. M. Saleh, *Saudi Pharm J.*, 2018, **26**, 64.
171 L. L. Li, J. H. Xu, G. B. Qi, X. Zhao, F. Yu and H. Wang, *ACS Nano*, 2014, **8**, 4975.
172 A. F. Radovic-Moreno, T. K. Lu, V. A. Puscasu, C. J. Yoon, R. Langer and O. C. Farokhzad, *ACS Nano*, 2012, **6**, 4279.
173 D. L. Slomberg, Y. Lu, A. D. Broadnax, R. A. Hunter, A. W. Carpenter and M. H. Schoenfisch, *ACS Appl. Mater. Interfaces*, 2013, **5**, 9322.
174 K. Ikuma, A. W. Decho and B. L. Lau, *Front. Microbiol.*, 2015, **6**, 591.
175 J. M. V. Makabenta, A. Nabawy, C. H. Li, S. S. chmidt-Malan, R. Patel and V. M. Rotello, *Nat. Rev. Microbiol.*, 2021, **19**, 23.
176 T. O. Peulen and K. J. Wilkinson, *Environ. Sci. Technol.*, 2011, **45**, 3367.
177 P. Meers, M. Neville, V. Malinin, A. W. Scotto, G. Sardaryan, R. Kurumunda, C. Mackinson, G. James, S. Fisher and W. R. Perkins, *J. Antimicrob. Chemother.*, 2008, **61**, 859.
178 D. Hu, H. Li, B. Wang, Z. Ye, W. Lei, F. Jia, Q. Jin, K. F. Ren and J. Ji, *ACS Nano*, 2017, **11**, 9330.
179 E. O. Mikhailova, *J. Funct. Biomater.*, 2020, **11**, 84.
180 C. R. Thorn, P. L. Howell, D. J. Wozniak, C. A. Prestidge and N. Thomas, *Adv. Drug Delivery Rev.*, 2021, **179**, 113916.
181 **https://apps.who.int/iris/bitstream/handle/10665/334216/9789240010789-eng.pdf**.
182 Q. Wan and T. J. Webster, *J. Biomed. Mater. Res.*, 2012, **100**, 3205.
183 H. A. Tran and P. A. Tran, *ACS Appl. Mater. Interfaces*, 2021, **13**, 41435.
184 R. Teixeira-Santos, M. Gomes, L. C. Gomes and F. J. Mergulhão, *iScience*, 2020, **24**, 102001.
185 H. Mohammed, A. Kumar, E. Bekyarova, Y. Al Hadeethi, X. Zhang, M. Chen, M. S. Ansari, A. Cochis and L. Rimondini, *Front. Bioeng. Biotechnol.*, 2020, **8**, 465.
186 S. Kumar, S. Raj, E. Kolanthai, A. K. Sood, S. Sampath and K. Chatterjee, *ACS Appl. Mater. Interfaces*, 2015, **7**, 3237.
187 S. Liu, T. H. Zeng, M. Hofmann, E. Burcombe, J. Wei, R. Jiang, J. Kong and Y. Chen, *ACS Nano*, 2011, **5**, 6971.
188 O. Akhavan and E. Ghaderi, *ACS Nano*, 2010, **4**, 5731.
189 S. Gündel, M. E. de Souza, P. M. Quatrin, B. Klein, R. Wagner, A. Gündel, R. A. Vaucher, R. C. V. Santos and A. F. Ourique, *Microb. Pathog.*, 2018, **118**, 268.
190 B. V. Worley, K. M. Schilly and M. H. Schoenfisch, *Mol. Pharmacol.*, 2015, **12**, 1573.
191 D. G. Meeker, S. V. Jenkins, E. K. Miller, K. E. Beenken, A. J. Loughran, A. Powless, T. J. Muldoon, E. I. Galanzha, V. P. Zharov, M. S. Smeltzer and J. Chen, *ACS Infect. Dis.*, 2016, **2**, 241.
192 B. Mai, M. Jia, S. Liu, Z. Sheng, M. Li, Y. Gao, X. Wang, Q. Liu and P. Wang, *ACS Appl. Mater. Interfaces*, 2020, **12**, 10156.
193 A. G. Ashbaugh, X. Jiang, J. Zheng, A. S. Tsai, W. Kim, J. M. Thompson, R. J. Miller, J. H. Shahbazian, Y. Wang, C. A. Dillen, A. A. Ordonez, Y. S. Chang, S. K. Jain, L. C. Jones, R. S. Sterling, H. Mao and L. S. Miller, *Proc. Natl. Acad. Sci. U. S. A.*, 2016, **113**, 6919.
194 K. K. Patel, D. B. Surekha, M. Tripathi, Md. M. Anjum, M. S. Muthu, R. Tilak, A. K. Agrawal and S. Singh, *Mol. Pharmacol.*, 2019, **16**, 3916.
195 J. Wang, X. Y. Chen, Y. Zhao, Y. Yang, W. Wang, C. Wu, B. Yang, Z. Zhang, L. Zhang, Y. Liu, X. Du, W. Li, L. Qiu, P. Jiang, X. Mou and Y. Li, *ACS Nano*, 2019, **13**, 11686.
196 M. Fumakia and E. A. Ho, *Mol. Pharmacol.*, 2016, **13**, 2318.
197 C. R. Thorn, A. Wignall, Z. Kopecki, A. Kral, C. A. Prestidge and N. Thomas, *ACS Infect. Dis.*, 2022, **8**, 841.
198 US National Library of Medicine. **ClinicalTrials.govhttps://clinicaltrials.gov/ct2/show/NCT01315691**(2018).
199 US National Library of Medicine. **ClinicalTrials.govhttps://clinicaltrials.gov/ct2/show/NCT02104245** (2018).